Utrecht University

Faculty of Geosciences

Department of Earth Sciences

Environmental Hydrogeology group

S.B.N.S

M.Sc. Thesis

'Effect of limited warming on residual oil-gas tar'

.

Stefanos Gkekas

Utrecht 2014

.

Supervisors:

Prof. S. M. Hassanizadeh, Utrecht University

J. van Leeuwen, Project Leader, S.B.N.S.

Acknowledgements

I would like to thank Majid Hassanizadeh and Johan van Leeuwen for their supervision, trust and support. I am deeply grateful to Nikos Karadimitriou for his contribution to my research. I would also like to thank Chiara Cassarini for her technical support. Last but not least, I owe a great debt of gratitude to my family, friends and colleagues for putting up with my bad mood during the long days of experimental work.

Contents

List of figures

List of tables

ABSTRACT

The potential of limited soil warming (50 °C) to function as a residual DNAPL phase remobilisation method, under the specific conditions of the 'Amersfoort Vetgasfabriek' site remediation project, is evaluated with this experimental study. The concept is based on the expected drop of NAPL-water interfacial tension with rising temperature. In order to maintain adequate correspondence of the experimental results to the actual field conditions, the materials used, i.e. oil-gas tar and sand, were collected directly from the particular site. Our measurements showed an approximate 40% drop of the tar-water interfacial tension with a rise of temperature from 15 to 50 °C. However the new equilibrium state established was more unfavourable as the DNAPL-water density difference drop is more significant for the specific temperature rise. The column experiments came to verify this result. Limited warming was applied on soil carrying residual tar saturation, condition created by consecutive drainage and imbibition phases. The entrapped DNAPL maintained its position in the sand pores despite the increased flow velocity of water during flooding at the elevated temperature. Limited warming was proven inadequate to function as a residual phase remobilisation method. Nevertheless, valuable insight was gained on the behaviour of the particular oil-gas tar during the drainage and imbibition cycles.

1. INTRODUCTION

1.1. Background

A significant number of soil and groundwater contamination cases pertain to the presence of non-aqueous phase liquids (NAPLs) in the subsurface. Mainly originating from anthropogenic spills on or directly below the soil surface (e.g. at industrial sites) the NAPLs migrate and may settle in the subsurface, persisting as a separate phase among the naturally present phases, i.e. groundwater and air in the vadoze zone and only groundwater in the saturated zone. Once the NAPLs are in contact with the groundwater phase, a slow yet continuous dissolution process begins which given the high toxicity of NAPL components becomes a long term groundwater contamination source.

In the case of dense NAPLs (DNAPLs), i.e. denser than water, the main direction of migration is downward regardless the zone the migration is occurring (vadoze or saturated). However, downward movement can be temporarily or even permanently halted when the migrating DNAPL comes across horizontal (or almost horizontal) planes of heterogeneity, resulting in pooling and additional horizontal spreading. These planes of heterogeneity can be either the groundwater table, i.e. heterogeneity of pore space saturation, or geological heterogeneities, i.e. porous medium heterogeneity.

Wettability is a fundamental property multiphase systems determining the configuration (saturation distribution) and overall behaviour (flow, entrapment, recoverability) of the fluid phases present in a particular porous medium [1]. Usually one of the fluid phases present (wetting phase) exhibits a stronger affinity for the grain particles. This phase is adhesively coating the grain surfaces, expelling the rest of the phases (non-wetting) towards the interior of the pore space [2]. However there are cases where none of the phases present exhibits a stronger affinity for the grains surface, resulting in a mixed wettability condition. Under normal conditions a virgin aquifer having experienced no previous contact with NAPLs is a water-wet system [3], [1]. This means that the DNAPL behaves as the non-wetting phase having to displace the wetting phase in order to advance (drainage process). Complete displacement of the wetting phase is not possible in this system as a wetting phase envelope remains around the soil grains.

The pattern of DNAPL migration below the groundwater table depends on the characteristics of the fluid phases (NAPL and water) and of the porous medium and is governed by the complex interplay of gravitational, viscous and capillary forces. After having penetrated the water table and with density higher than water, the DNAPLs continue their downward movement displacing water from the soil pores. DNAPL advancement can occur either in a stable pattern (stable front) or in an unstable pattern (fingering) depending on the NAPL potential to displace the water phase [4] [2], [5].

As DNAPL drains through the soil pores driven by gravity, traces of residual phase are left behind entrapped. This immobilisation-entrapment occurs when water phase (wetting) imbibes back in the pore space previously occupied by the advancing DNAPL phase (non wetting). Two main trapping mechanisms are identified: by-passing and snap off. The resulting entrapped non-wetting phase can be isolated, discrete and amorphous blobs or ganglia of a variety of shapes. [2], [6], [3]. The residual NAPL saturation can vary widely, but typically amounts a 15-30% of the total saturation. From a macroscopic viewpoint, residual saturation is rarely uniformly distributed.

In most cases only some areas containing entrapped NAPL contribute significantly to the total fraction of NAPL saturation compared to the rest of the total pore volume. [3]

NAPL residual saturation functions as a persistent source of groundwater contamination as it tends to hold its place in the soil pores surrounded by the continuous water phase in the long term producing contaminants' concentration in groundwater via slow dissolution. The latter is enhanced by the higher interfacial area over respective volume ratio of the residual NAPL phase compared to the continuous NAPL phase. NAPL phase entrapment is a major hindering factor for remediation. NAPL residuals remain unaffected by pressure gradients within the normal in-situ applicability range causing conventional NAPL phase removal methods to fail, e.g. hydraulic removal. [6] The implementation of additional remediation techniques based on micro-scale physics is necessary in order to overcome the entrapment conditions and mobilise residuals creating thereby the required conditions for efficient removal.

The discontinuous NAPL bodies are not able to exert a capillary pressure higher than the entry capillary pressure at their advancing front; as a result they remain immobile. The capillary pressure builds up as a result of the system driving forces, which can be viscous due to flow of the surrounding water phase and/or gravitational due to the density difference between the fluids. These driving forces are opposed to the resisting capillary forces developed at the pores constrictions as a result of the fluid-fluid interfacial tension as a function of wettability, contact angle, pore geometry and heterogeneities.

Depending on the system configuration only one of the two or both the driving forces can be present. Viscous forces develop in the direction of the wetting fluid flow. In a system with no density difference between the fluid phases or in the direction of flow perpendicular to gravity only viscous forces are present. The latter are related to the resisting capillary forces via a dimensionless ratio, the Capillary number:

$N_{ca} = \frac{q\mu}{\gamma \cos\theta}$ [7], where q: Darcy velocity [L/T], μ: viscosity of the displacing fluid [FT/L^2], γ: interfacial tension [F/L] and θ: contact angle [7]

In the case of stagnant wetting phase and given that a density difference between the two phases applies, the only driving force of the system is gravity. The latter is related to the resisting capillary forces via a second dimensionless ratio, the Bond number:

$N_b = \frac{g\left|\rho_w - \rho_n\right| l^2}{\gamma \cos\theta}$ [7], where g: gravitational acceleration constant [L/T^2], ρ_w and ρ_n: wetting and non-wetting phase densities [M/L^3], l: characteristic pore size [L], γ: interfacial tension [F/L] and θ: contact angle[7]

In the case that both driving forces are present, i.e. there is density difference between the phases and the surrounding wetting phase is flowing in a direction other than perpendicular to gravity, then the two driving forces can be superimposed. The effect of viscous and gravitational forces against capillary forces can be combined in a direct summation of Capillary and Bond numbers [8], [4]. For a single pore which a NAPL globule is entrapped as idealised by the pore snap-off model (see Figure 1.1) and for flow direction aligned to gravity, a total trapping number (NT) is expressed as the sum of the capillary and Bond numbers: $N_T = \left|N_{Ca} + N_B\right|$

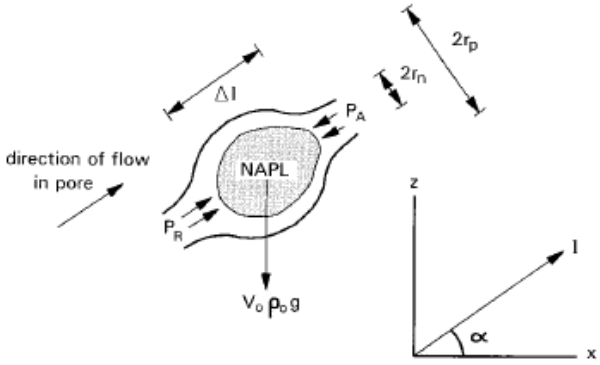

Figure 1.1: Schematic diagram of the pore entrapment model and corresponding coordinate system [8]

In order for entrapped NAPL re-mobilisation to occur, the capillary pressure at the NAPL water interface (drainage front) must exceed the entry pressure of the pore constrictions. This can happen either by increasing the capillary pressure at the NAPL-water interface or by decreasing the entry pressure at the pore constriction. Increase of the capillary pressure can be achieved with an increase of the driving forces of the system.

An increase of the viscous forces resulting from an increased wetting phase flow rate can be expressed by a rise of capillary number. In this case the pressure gradient of the flowing wetting phase must become high enough to squeeze the residual NAPL blobs through the pore constriction. However, this attempt is hindered by the complexity and dynamic character of the phenomenon and the resulting increased capillary pressure is not analogous to the increase of the wetting phase pressure gradient. Depending on the system, there is a critical capillary number that must be reached in order to induce instability. The order of magnitude of the critical capillary number reported in literature varies from 10^{-5} to 10^{-2}. These capillary numbers correspond to unrealistic flow rates for normal aquifer flow rates. The amount of residual saturation reduction by hydraulic mobilisation can strongly depend on the distribution of the entrapped pore bodies in the pore scale. Long and complex ganglia formed by bypassing can be easier mobilised than singlet blobs caused by snap-off because a greater pressure difference can be easier established along them. [9], [7], [6]

An increase of the gravitational forces results from an increase in the density difference between the phases. This increase in density difference leads to a direct increase of capillary pressure at the NAPL water interface and can be expressed by an increase in Bond number. However, due to the entrapment process, the capillary pressure at the drainage front of an entrapped NAPL body may be well below the entry pressure of the pore constriction. Hence a significant increase in density difference is required to overcome the entry pressure and allow the NAPL phase to drain through the constriction. Even if the required capillary pressure is reached allowing the NAPL to advance, it is most likely that a secondary entrapment mechanism will develop causing a part of the NAPL body to separate and remain entrapped.

Reducing the entry pressure may result from a drop in the interfacial tension between the phases or intervention on the wettability of the system (change of contact angle). A drop in the interfacial tension can be achieved with increasing temperature [7] or with the use of chemicals (surfactants). The wettability of the system can be manipulated for example with change in pH

[10]. Finally, NAPL remobilisation may be achieved with a direct intervention in the pore structure, for example with vibration or freeze-thaw cycles. [11],[12]

1.2. The case

The present study is based on the contamination case of the site "Old Pintsch gas factory" located in Amersfoort, The Netherlands. At this site the presence of an aged multi-component NAPL mixture in the subsurface, generally behaving as DNAPL (oil-gas tar, also named "Amersfoort oil"), functions as a source of severe groundwater contamination [13]. The hydrogeological setting consists of a phreatic sandy aquifer of approximately 9 m saturated thickness with a 3 m unsaturated zone, bound from the lower sandy (confined) aquifer layers by a peat-on-clay thin aquitard layer. The oil-gas tar NAPL produced during the Pintsch gas manufacture (process of oil thermo-cracking in steam environment) was disposed near the surface[1] more than 60 years ago and after migrating downwards through the phreatic aquifer it has pooled on the aquitard layer. During downward migration a significant amount of NAPL was left behind in the form of trapped-residual saturation forming a huge immobile NAPL saturation zone located on top of the mobile NAPL pool. The present situation is illustrated in Figure 1.2, below.

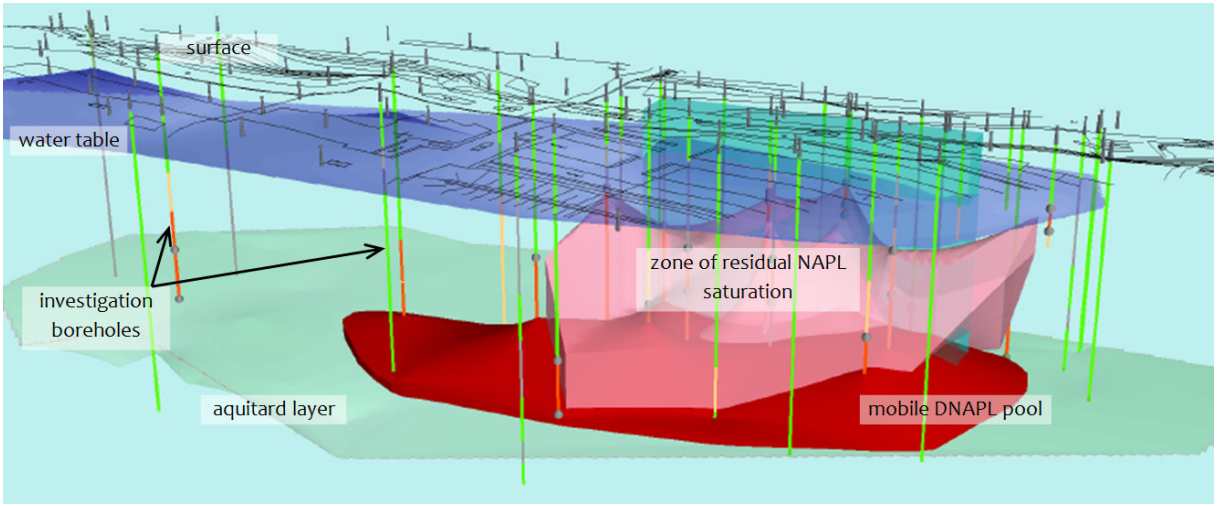

Figure 1.2: Contamination situation at the Amersfoort site [14]

The remediation plan consists of two parts. The first part is the removal of the mobile phase NAPL by pumping; the second part is the treatment of the zone carrying residual phase NAPL. Especially the treatment of residual zone is an extremely complex problem requiring a well targeted, site specific and integrated remediation plan. One of the methods under consideration is the application of limited warming.

Limited warming is a term used to describe the continuous warming of the soil to the constant temperature of 50°C. The word limited is used to distinguish this level of warming from the remediation methods heating the soil up to the boiling point of the NAPL and other techniques mostly used in the petroleum industry such as steam flooding, in situ radio frequency heating,

[1] Disposal conditions are not fully known

joule resistance heating and hot water flooding [7] . This level of warming, i.e. up to 50°C, can be sustained in field conditions in a relatively energy and cost effective manner. Heat is transferred to the soil via an array of warming elements. Those elements are spiral pipes installed in the soil at the desired depth range, circulating warm water in a closed system. Circulation of warm water is conducting heat to the soil and pore fluids causing the temperature of the subsurface to rise. The application of limited warming is part of the remediation plan related to the removal of free phase NAPL (pool zone). Taking advantage of the significant effect of temperature on the viscosity of the particular NAPL (see Figure 2.5) limited warming is expected to enhance mobile NAPL recovery.

Since limited warming will be applied at the lower zone of the aquifer (pool zone-mobile NAPL phase) the possibility to apply limited warming as a method for the remediation of the residual NAPL saturation zone was considered. This extension can be easily achieved simply by adding a second warming element at the depth range of the residual NAPL saturation zone, i.e. on top of the pool zone. The effect of limited warming on both zones will be tested at a pilot field test. The installation concept is given in Figure 1.3.

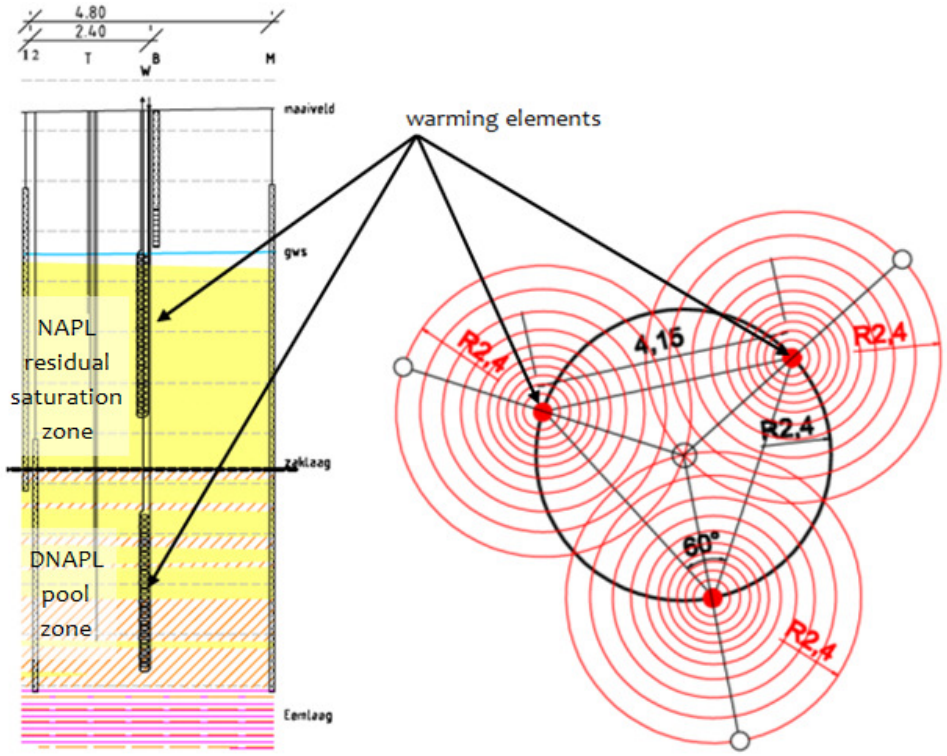

Figure 1.3: Array of warming elements for pilot field test (left cross-section, right plan view)

The application of warming is the same for the two zones; however the remediation principle is different. The target of limited warming for the mobile NAPL saturation is the viscosity of the flowing DNAPL phase (see Figure 2.5). The target for the residual NAPL saturation is the interfacial tension between the NAPL and water phases.

Interfacial tension is one of the critical parameters in a system where one of the two fluid phases is at residual saturation. It is responsible for holding the isolated DNAPL blobs or ganglia perched opposed to gravity. Assuming that wettability within this range of temperature variation (from in situ temperature of approx. 15 °C to 50°C) remains unaffected, based on the expected reduction of interfacial tension with warming the entry pressures at the pore constrictions are decreased

[7]. Thereby the equilibrium state of trapped NAPL phase is disrupted allowing the system to switch to a new equilibrium.

Apart from the reduction of interfacial tension raising temperature has an effect on the density of phases. Based on that, it is not clear whether the overall effect will be positive, since the favourable decrease of interfacial tension and corresponding capillary forces may be counteracted by an unfavourable change in density difference and corresponding gravitational forces. [7]

The question is whether (and if yes to what extent) the transition to this new equilibrium can trigger the re-mobilisation of the entrapped NAPL phase. It was decided that the most efficient way to get a clear and direct answer was to test the method on the particular site conditions. Apart from the above described pilot scale field application, it was decided the effect of limited warming on residual NAPL saturation should be investigated in depth with additional laboratory research.

1.3. The research

The present study is the experimental research performed to evaluate the potential of limited warming to function as a re-mobilisation factor for the site-specific conditions of residual DNAPL (oil-gas tar) saturation. To this end, the entire research was designed and carried out based on the in-situ conditions encountered at this particular site, i.e. the particular DNAPL type existing as an entrapped phase in the particular sandy porous medium. The aim was to build a laboratory scale simulation of the method in order to provide the means for proper investigation of the physical process, i.e. the effect of limited warming on the NAPL entrapment conditions, while maintaining adequate correspondence to the actual in-situ conditions of that particular remediation site.

In order to simulate the application and effect of limited warming on the in situ conditions in an efficient manner it was first necessary to look into the process as it would happen in the field. This process can be simply outlined as a perturbation of a system in equilibrium aiming at a specific result. The system is the zone of the particular aquifer carrying residual-immobile saturation of the particular NAPL (see Figure 1.2), in other words a porous medium whose pore space is fully occupied by two liquid phases. One of those phases (NAPL) is at residual saturation while the other phase (water) occupies the rest of the pore space. As the NAPL phase is immobile the particular pore space partitioning is in equilibrium. The perturbation is the transition from the constant in situ temperature (approx. 15 °C) to a new constant temperature level, that of limited warming (50 °C). The experimental research was built exactly on this path. First, the in situ equilibrium conditions were reproduced. These conditions were investigated separately aiming to provide insight on the behaviour of the system. With this as a starting point, the perturbation of the system was applied and the result was evaluated.

2. MATERIALS & METHODS

2.1. Materials

In this section the design of the experimental setup and materials are presented. Furthermore, a brief listing of the equipment used for the experimental purposes is provided.

a. Experimental setup

The experimental setup was designed according to a series of requirements. The experimental scale should satisfy the needs of the particular research. As the target of this experimental research was to interfere with the NAPL entrapment conditions at the pore scale, a total volume containing sufficient number of pores could be regarded as Reference Elementary Volume (REV). In this way, the macroscopic dimensions of the system are much larger than the microscopic characteristic length.

Furthermore, in order to achieve adequate correspondence to the field conditions, the experimental scale was expanded to Darcy scale. The first reason for this expansion was that based on field observations the entrapped NAPL bodies can occupy a significant number of consecutive pores even though the equilibrium state is controlled in the pore scale. The second reason was the intention to allow the experimental scale to contain sufficient number of pore network heterogeneities. On the other hand an upper limit applied to the experimental scale for functionality reasons.

As the aim of this research work was to investigate the effect of warming on the equilibrium conditions between gravity and interfacial tension, the main axis of the experimental setup was aligned with gravity. Furthermore with an axisymmetric shape the distance and effect (e.g. unwanted drainage paths, heat transfer) of the side boundaries was kept uniform in regards to the central axis of the setup. Based on those two requirements, i.e. verticality and axisymmetry, cylindrical columns were chosen to contain the porous medium.

The main operational requirement which the column design should satisfy was the circulation of fluids along the vertical axis through the porous medium (drainage, imbibitions phases). This circulation of fluids should be either pressure or flow driven. Accordingly, the top and bottom boundaries of the system, i.e. the porous medium, should be such that these conditions could be applied and modified depending on the phase of the experiment. In particular, at the top boundary a pressure boundary condition should be applied. The method to apply this pressure was by ponding particular height of fluid phase on top of the porous medium. As this pressure should be applied uniformly on the upper surface of the porous medium the top part of the column did not contain sand (porous medium) but was reserved for fluid ponding. In the case that the needed pressure would exceed the maximum fluid height in the column, additional ponded height should be provided by a pressure tube mounted on the top of the column. The bottom boundary of the porous medium coincided with the bottom boundary of the column. At that level both pressure and flow boundary conditions should be applied. The pressure boundary condition should switch between the atmospheric pressure (boundary open-flow condition) and

the static pressure of fluids (boundary closed-no flow condition). For the flow boundary condition fluids should be able to be injected or extracted.

As for the materials used, these should be inert (unreactive) to the experimental fluids and adsorb the least amount of NAPL components.

In order to satisfy the experimental requirements, the experimental setup consisted of the following parts:

- Plexiglas (Polymethylmethacrylate-P.M.M.A.) columns of internal diameter (I.D.) of 8cm, wall thickness of 5mm and height 14,6cm were used to contain the sand and experimental liquids.
- Top and bottom ends of the cylindrical columns were closed with Teflon (Polytetrafluoroethylene-P.T.F.E.) lids and sealed with o-rings. The o-rings seals were constrained between the inner wall of the column and the outside surface of the lids.
- Both lids carried mounted brass valves at their centre for inlet/outlet of fluids. The top valve (inlet) was female to male of I.D. 10mm, with the male end mounted in the top lid. The bottom valve (outlet) was a male to male of I.D. 8mm.
- A 50cm transparent tube (pressure tube) was mounted in the female (top) side of the top valve for application of fluid pressure on top of the column.

The experimental setup is shown in Figure 2.1.

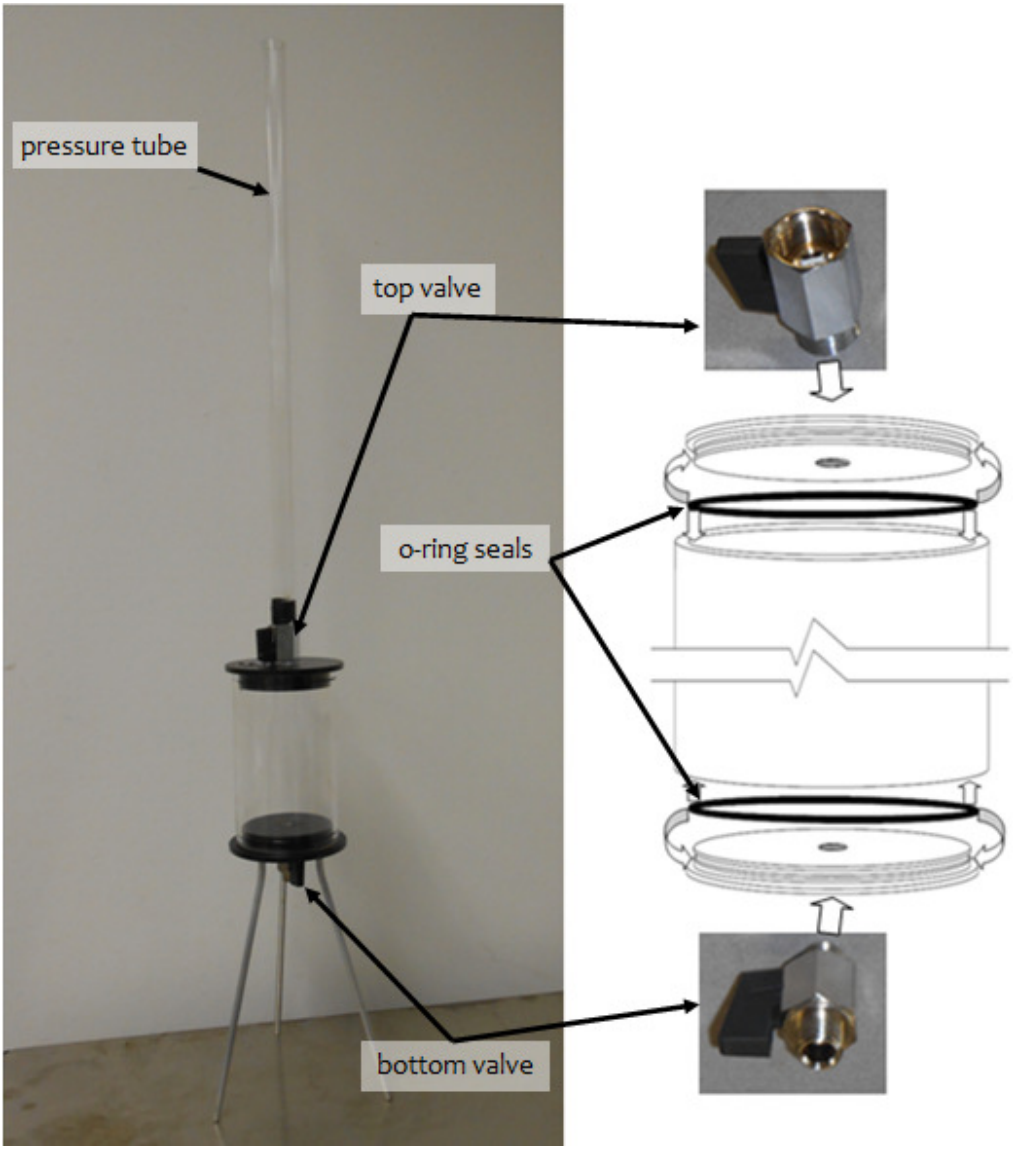

Figure 2.1: Column setup consisting of: a. Plexiglass (P.M.M.A.) column, b. Top and bottom Teflon (P.T.F.E.) lids, c. O-ring seals, d. Top (inlet) and bottom (outlet) brass valves, e. Pressure tube and f. Supporting legs

Note: Initially glass columns (hydrophilic) were used instead of the above described Plexiglas (organic) columns. However in the particular setup design the lids were sealed at the inner side of the columns. Due to warming, the thermal expansion of the lids and the O-ring seals applied radial pressure at the interior of the cylindrical column. This produced tensile circumferential stresses on the column wall. Glass, i.e. of the particular thickness used, was proven of insufficient tensile capacity to handle those tensile stresses and failed. For this reason the experiment was re-designed using Plexiglass material for the columns.

b. Porous medium

In order to create a representation of the in situ conditions in the columns, sand collected directly from the Amersfoort site was used as the porous medium of the experiments. In particular, sand was taken from the residual NAPL saturation zone, i.e. from the path that DNAPL migrated through in the past leaving behind trapped immobile saturation. In Figure 2.2 the overall field

contamination situation is given. The zone currently carrying residual NAPL saturation exists on top of the huge and laterally spread mobile saturation zone (DNAPL pool zone).

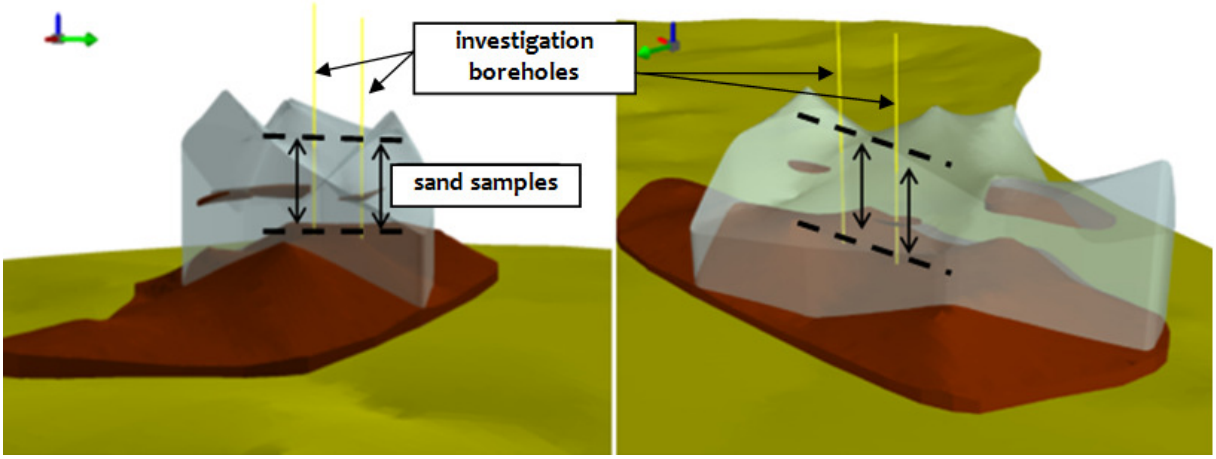

Figure 2.2: Amersfoort site contamination situation (West domain). Green: aquitard layer, dark red: mobile D.NAPL pool, transparent white: residual D.NAPL zone and yellow: investigation boreholes (A033son2 and A034son2) [14][13]

Sand samples were chosen from the sonic drilling cores extracted from the two boreholes shown in Figure 2.2. Representative parts of the two cores are shown in Figure 2.3.

Figure 2.3: Representative sonic drilling cores containing immobile NAPL saturation [14][13]

Figure 2.4: Sand samples used in the experiment

c. *Experimental Liquids*

Similarly with the porous medium, the NAPL phase used in the experiments was oil-gas tar existing in the subsurface of the Amersfoort site. It consisted of the saturation carried in the sand samples, hereafter named S^{i}_{NAPL}, plus additional free phase DNAPL pumped out directly from the mobile pool zone of the Amersfoort site (see Figure 2.2). The composition and physical properties of the multi-component free NAPL phase were defined from laboratory measurements prior to the present experimental study on samples collected from the same borehole filter as the free phase DNAPL used in the present experiment. Density at 15°C was measured at 1.0308 g/ml. The composition is given in Table 2-1 and the dynamic viscosity variation with temperature in Figure 2.5.

Compound group %		Carbon fraction %	
Volatile aliphatic	3.9	Benzene	0.0
Non-volatile aliphatic	0.0	Toluene	0.01
Volatile aromatic	5.4	Ethylbenzene	0.1
Non-volatile aromatic	8.3	Xylene	0.4
2-Ring polycyclic	16.4	C6-C10 total	9.3
3-Ring polycyclic	27.2	C10-C12	10.5
>4-Ring polycyclic	19.3	C12-C16	34.5
Heterocyclic N-	12.1	C16-C22	24.4
Heterocyclic S- & O-	1.6	C22-C30	15.9
Anilines & Phenols	0.0	C30-C40	5.5
Oxidised	5.9	C10-C40 total	90.7
Orgenic acids	0.0	Total tar C6-C40	100

Table 2-1: Oil-gas tar (NAPL) composition [14][13]

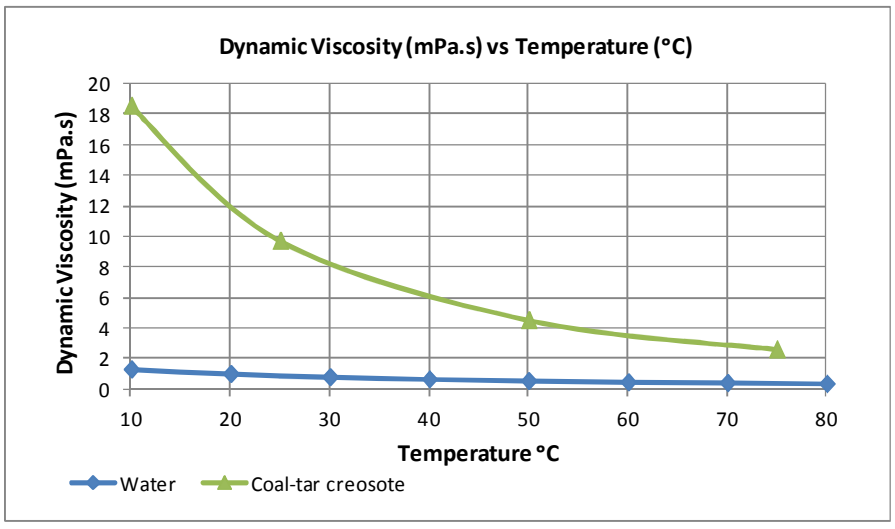

Figure 2.5: Free phase oil-gas tar variation of dynamic viscosity with temperature. Dynamic viscosity of water is given as reference.

Tab water was used in all the phases of the experiment. This choice was based on the fact that water circulation should be implemented during most of the phases of the column experiment, therefore requiring excessive amounts of water. Using contaminated water collected from the field would require additional equipment and would complicate the experimental procedure considerably.

d. Equipment

The equipment used in the different phases of the experiment is briefly presented in the following listing. The use of each piece of equipment is provided in Section 2.2 with the respective method description.

- Optical setup consisting of GC2405 Ethernet camera combined with Sonnar 1.8/a35 ZA lens was used to capture photographic profiles of sessile and pendant drops. For the pendant drops a top-side open glass cube with a perforated cap and a needle with I.D. of 0.5 mm were used. (Figure 2.6.a)
- A warm water bath with silicon tubing was used to alter the temperature conditions in the column. The warm water bath carried its own pump. (Figure 2.6.b)
- A warming plate was used for warming liquids for tests and measurements performed parallel to the column experiments (Figure 2.6.c)
- A three decimal digit scale was used for all gravimetric measurements (Figure 2.6.d)
- For fluid circulation through the columns a peristaltic pump with silicon tubing was used (Figure 2.6.e)
- Thermocouples, a data logger (Figure 2.6.f) and a notebook were used for temperature control.
- Hydrophilic filters of 3mm thickness and average pore size 80-130μm were used for NAPL-water separation.
- Pure phase CO_2 was used to displace air phase from the sand during the saturation phase.
- H.D.P.E. sample bottles of 250ml were used for the collection of liquid experimental products.
- Two glass syringes of 5 and 10 ml with Luer lock were used to handle liquid amounts during different phases of the experiment.
- Glass laboratory vessels were used as reservoirs during different phases of the experiment.

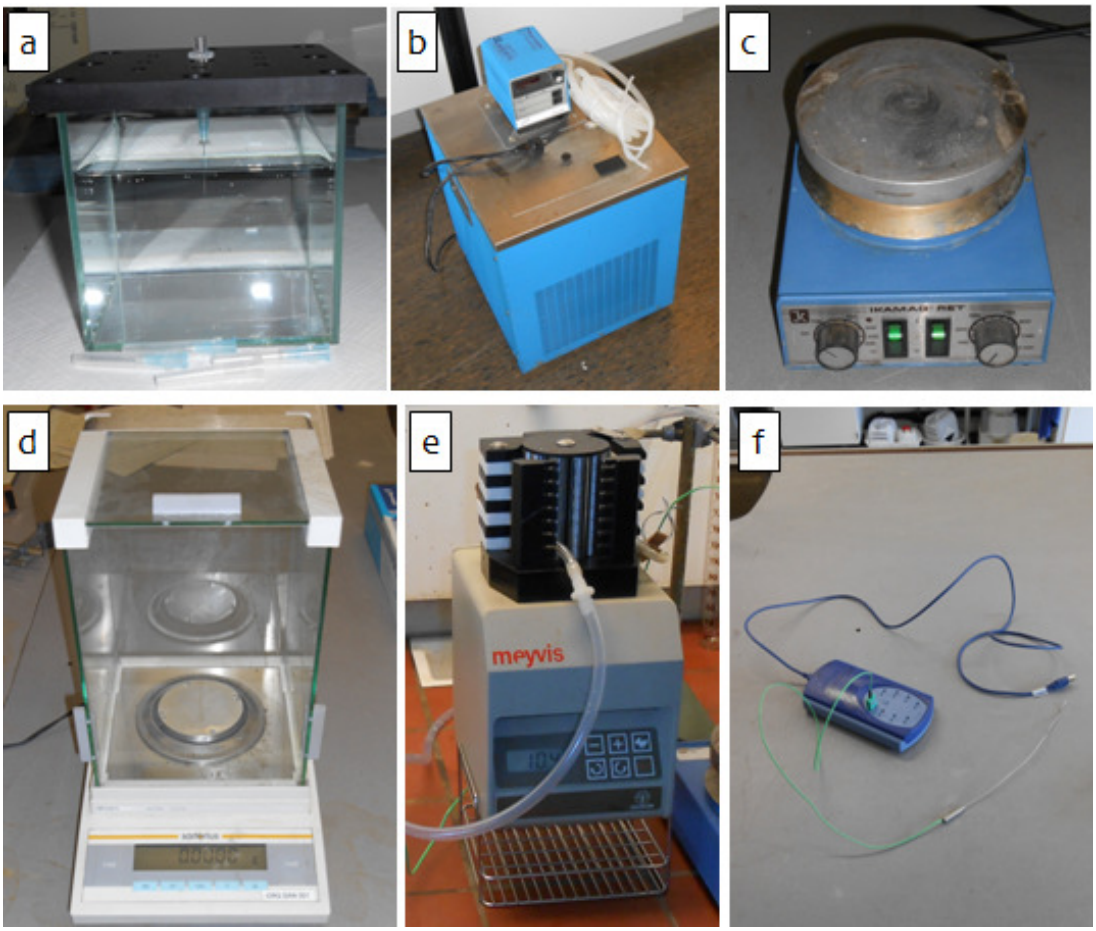

Figure 2.6: Equipment; a: glass cube, b: warm water bath and silicon tubing, c: warming plate, d: scale, e: peristaltic pump and f: thermocouple and date logger

2.2. Methods

Within this chapter the experimental procedure followed is analysed. Apart from the main column experiment a series of parallel tests and measurements was carried out in order to integrate the experimental research. This additional set of actions was necessary firstly in order to determine properties and behaviour of the system's components both individually but also interacting. Secondly it provided the means for proper quantification of the experimental results. The experimental procedure was therefore divided into three major series of actions which were executed independently:

1. System investigation
2. Column experiment
3. Measurements

The above groups of actions are presented separately within sections 2.2.1, 2.2.2 and 2.2.3.

2.2.1. System investigation

Within the system investigation the actions performed parallel to the main column experiment in order to determine the properties and behaviour of the system are included. This additional investigation was necessary because the materials used in the experiment were non-standardised and therefore of partly known properties and behaviour. In that context the following series of tests and measurements were performed:

a. Wettability test of the sand-water-NAPL system.
b. Measurement of NAPL density and variation with temperature.
c. Measurement of interfacial tension between water and NAPL and variation with temperature

a. Wettability

A separate test was performed in order to determine which of the two phases present, i.e. water or NAPL, is preferentially wetting this specific porous medium. The test applied the "sessile drop" static contact angle principle [1], a simple yet reliable method to determine the wettability, according to the following.

The test was carried out at ambient laboratory temperature (21 °C). It was assumed that within the particular range of temperature variation of the present research (15 to 50 °C) the wettability of the system remains practically unaltered. A smooth sand surface was created in a rectangular batch. The space above the sand surface was covered by water. A droplet of NAPL formed below the water surface from a syringe needle was placed on the medium surface surrounded by the background water phase. The created sessile drop was allowed to age for 5 hours in order to be regarded as stable before photographic profiles were taken. Based on the contact angle at the intersection of sand, water and NAPL the wettability of the system was determined. No direct measurements of the contact angle were performed; the conclusion was based simply on

whether the contact angle θ would be >90°+ψ or <90°-ψ [2] corresponding to NAPL or water wet system respectively [2][1]. The sessile drop principle is given in Figure 2.7.

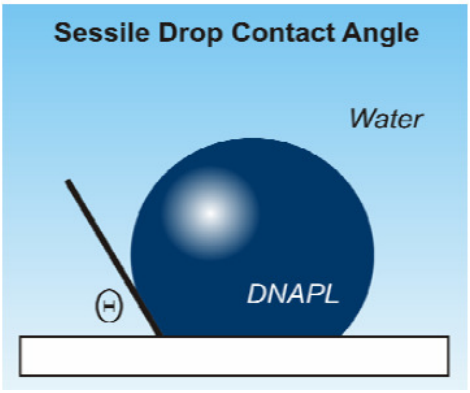

Figure 2.7: System wettability based on contact angle θ of sessile drop [1]

b. Density

The density of the NAPL was measured at 15°C during earlier laboratory tests related to the particular soil remediation project. For the purposes of this experiment however the density of the NAPL was defined for the whole temperature range of 10°C to 50°C. The method followed consisted of density measurements at different temperature levels and subsequent interpolation in a $\rho_{NAPL} = f(T)$ curve. This curve was thereafter used to calculate density at any temperature point within the 10°C to 50°C range.

Apart for the first measurement at ambient laboratory temperature (21°C), three more measurements at 30, 38, and 48 °C were performed. The NAPL contained in a glass laboratory vessel was brought and kept at each of the higher than the ambient level temperature points using a warming plate. Temperature in the vessel was monitored using the thermocouple-data logger apparatus (see 2.1.d). The vessel with the thermocouple is shown in Figure 2.8.

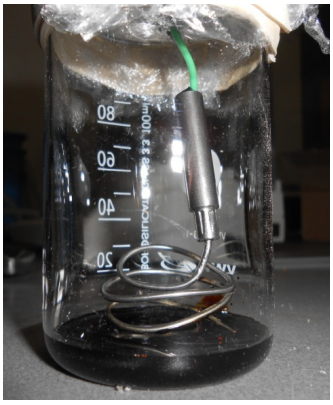

Figure 2.8: Glass vessel containing NAPL and thermocouple for measurements at different temperatures

[2] ψ: tolerance level around 90°, equal to 20° [1]

Density was measured using a syringe and the three-digit scale (see 2.1.d). Samples of the NAPL at the specific temperature were extracted from the vessel using the syringe. The N.A.P.L density was calculated by weighing the syringe first containing the initially extracted amount of NAPL and second after expelling specific volumes (0.5 and 1 ml) from the syringe. The density of the NAPL was calculated by dividing the weight difference with the respective volume of expelled NAPL. Measurements were repeated for different samples at the same temperature to eliminate errors.

Density of water at different temperatures was similarly calculated based on a $\rho_{water} = f(T)$ curve provided by literature source. [15]

$$\rho_W(g/cm^3) = \frac{1-(T(°C)+288.9414)}{508929.2*(T(°C)+68.12963)*(T(°C)-3.9863)^2}$$

c. *Interfacial tension*

Interfacial tension between water and NAPL phase was determined based on the method of pendant drop. This method is using the shape and dimensions of pendant drops to calculate interfacial tension. The pendant drops are created by injecting NAPL at some depth in the water phase. According to "the Method of Selected Plane" in particular, analysed by Tucker [16], the interfacial tension at the phase boundary can be calculated with high precision from photographic profiles of pendant drop and the density difference between the two phases.

The combination of pressure discontinuity, boundary tension and curvature of a liquid surface leads to the fundamental Young-Laplace equation which applies to any free, homogeneous fluid interface, irrespective of whether it is a liquid/liquid or liquid/gas interface, provided only that the surface is in static equilibrium.

$p = \gamma \cdot (1/R + 1/R')$ (Young-Laplace equation) (1)

where: p: pressure difference between the two sides of the surface, R and R' principal radii of curvature and γ: boundary tension (or free boundary energy)

Equation (1) links the pressure difference between the two sides of the interface with its boundary tension and its mean curvature and by assuming perfect symmetry the vertical forces acting across a horizontal plane are balanced leading to the famous:

$\Delta p = 2 \cdot \gamma / R$ (2),

which suited for the shape of the pendant drop is expressed as:

$\gamma = \Delta\rho \cdot g \cdot R_0^2 / \beta$ (3) [16][17]

where Δρ: mass density difference between the drop and the surrounding medium, g: gravitational constant, R_0: radius of curvature at drop apex (see Figure 2.9) and β calculated from the shape parameter σ :

$\sigma = \frac{D_S}{D_E}$ (4) , where D_E: equator diameter (size parameter – see Figure 2.9)

according to the following:

$$\beta = 0.12836 - 0.7577 \cdot \sigma + 1.7713 \cdot \sigma^2 - 0.5426 \cdot \sigma^3 \qquad (5) \qquad [17]$$

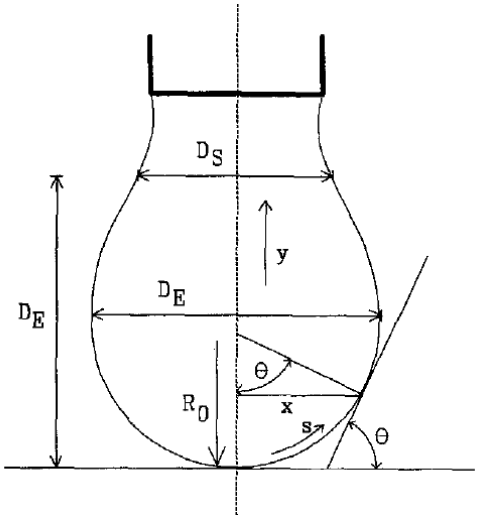

Figure 2.9: Geometry of pendant drops with variables [17]

Since the focus of the present study was the interaction of phases at different temperatures, a complete answer could not be provided simply by the measurement of interfacial tension at a particular temperature level. Hence, the measurements were repeated at different temperatures (16°, 22°, 30°, 38°, 49°C), ranging from a low boundary of approximately the in situ temperature (16° C) up to a maximum of 50°C, with the later being the upper boundary of what in this study is regarded as limited warming (see Section 1.2). This was managed by bringing both phases at the same temperature by warming (or cooling) in separate vessels: water in the glass cube (see 2.1.d) whereas NAPL in the same vessel used in the NAPL density measurements (see Figure 2.8). Warming was achieved using the warming plate (see 2.1.d), while cooling using ice in contact with the vessel or glass cube containing the materials. Temperature was controlled in both cases with thermocouples submerged in the liquids and the data logger (see Figure 2.8Figure 2.10). Once temperature was stabilised at the desired level a small volume of NAPL was extracted with a syringe from the vessel in order to produce the pendant drops.

The pendant drops were produced using the setup shown in the following Figure 2.10.

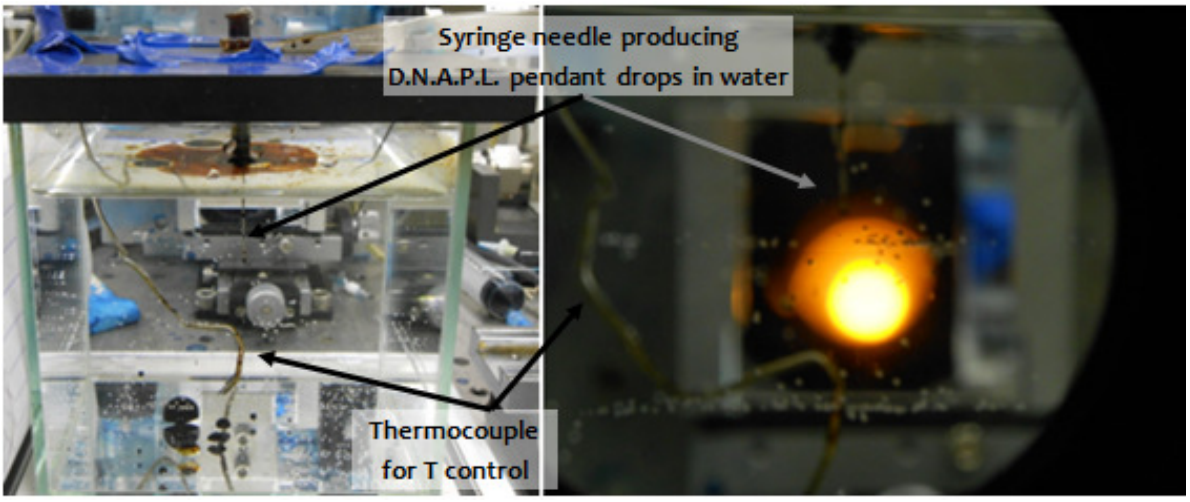

Figure 2.10: Setup used for the production of pendant drops

The DNAPL was injected in the water phase to create the pendant drops from the syringe tied at the top of a needle. The latter was fixed at the perforated cap of the glass cube (see Figure 2.6.a and Figure 2.10). Injection was executed in small pressure increments in order to assure that the pendant drops would equilibrate after each increment. The very last equilibrium before the release of the pendant drop from the lower edge of the needle due to own weight provided the maximum stable pendant drop suspended against gravity.

Photographic profiles of the pendant drops were taken with GC2405 Ethernet camera combined with Sonnar 1.8/a35 ZA lens every 100 msec in order to achieve the best possible resolution at the equilibrium point. The setup is shown in Figure 2.11.

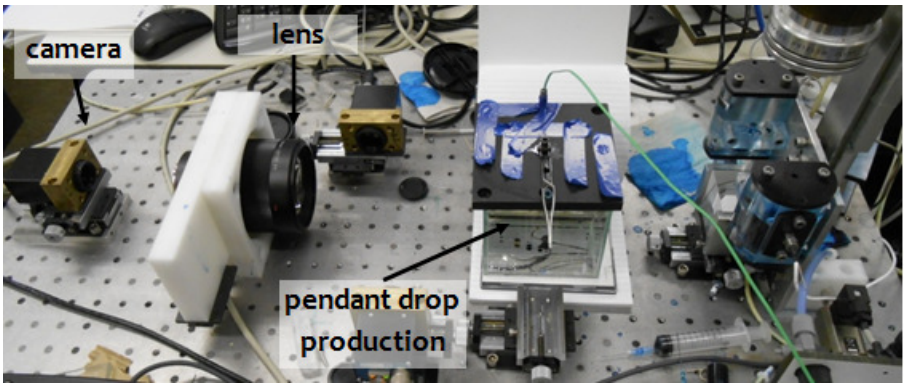

Figure 2.11: Complete setup for the application of the pendant drop method

An example of the produced pendant drop photographic profile shown in Figure 2.12.

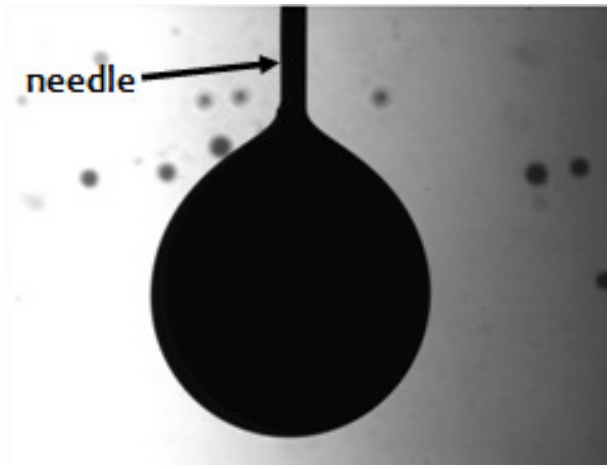

Figure 2.12: Example of pendant drop photographic profile

The pendant drop dimensions were extracted according to Figure 2.9 for the calculation of interfacial tension.

2.2.2. *Column experiment*

The main part of this work is the column experiments. The aim was to simulate the application of limited warming (see 1.2) on the in situ immobile NAPL saturation conditions.

The system, consisting of the porous medium and the two liquid phases (see Sections 2.1.b and 2.1.c), was first brought to the desired residual/immobile NAPL saturation. This first phase of the experiment was carried out at a constant temperature of 21 °C (ambient laboratory temperature), although ideally the temperature should match that of normal in situ conditions (approx. 15 °C). This choice was made for technical reasons and assuming firstly that the residual NAPL phase created at 21 °C would not differ from that created at 15 °C and secondly that the evaluation of the warming effect would be adequate even from a slightly elevated starting point.

Then limited warming (50°C) was applied. Apart from limited warming and in order to gain a better insight on the overall temperature effect, the experiments were extended to include temperature restoration at 21°C and cooling at 12°C.

The column experiments procedure consisted of the following three consecutive phases:

1. Preparatory phase
2. Creation of residual NAPL saturation condition
3. Temperature variation phase

The experiment was performed twice in order to verify the results and establish solid conclusions on the temperature effect. First, the standard experimental procedure was followed for the main experiment, hereafter referred to as **column 1 (C1)**, and then with some minor changes during phases 2 and 3 for the duplicate experiment, hereafter referred to as **column 2 (C2)**. In the following paragraphs the experimental phases are analysed and the differences between the

main and duplicate experiments (columns 1 and 2 respectively) are specified. Where no difference is specified the experimental procedure followed was identical.

a. Preparatory phase: Sand Homogenisation, packing and saturation

The sand samples described in Section 2.1.a were homogenised in a laboratory vessel. The final level of homogenisation produced from this method could not possibly reach that of standardised sand for laboratory use. However a decent end result was achieved in regards to the scale and nature of the experiment. As discussed in Section 2.1.a the intention was to allow pore network heterogeneities to develop in order to achieve a reasonable representation of the in-situ conditions.

As the natural variation of sand density in field conditions is impossible to reproduce in the laboratory it was chosen to neutralise that parameter using a constant average macroscopic density. Packing of sand in the columns was set at 1.8 g/cm^3, corresponding to an ordinary unit weight of shallow unsaturated normally consolidated sand deposits, i.e. 18 kN/m^3. Sand was packed in columns 1 and 2 following the exact same method, aiming at creating two identical and therefore comparable porous media. Height of sand was set at eight centimetres and packing was executed in 4 steps of two centimetres in order to control the macro-scale homogeneity of the porous medium. The relevant calculation is given below.

$$\left.\begin{array}{l}\rho_{sand}^{unsat}\,1.8\,gr/cm^3\\ h_{sand}=8cm\\ D_{column}=8cm\end{array}\right\}\rightarrow W_{sand}^{tot;column}=h_{sand}*A_{column}*\rho_{sand}^{unsat}=723.8\,g/column$$

$$n=4\rightarrow W_{sand}^{i}=\frac{W_{sand}^{tot;column}}{n}=180,95\,g/step$$

The above described procedure produced a 3-phase system, i.e. containing water, NAPL and air. For the purposes of the experiment this system was converted to a 2-phase, i.e. with only water and NAPL phases present. This was achieved following a 2-step method. First, air phase was eliminated from the sand pores by a thorough 4-hour per column low pressure bottom-top CO_2 injection. In this way the heavier CO_2 gradually displaced all the air contained in the column producing a new 3-phase system, with the gas phase being the fully miscible in water CO_2 instead of air. The CO2 injection procedure is shown in Figure 2.13 below.

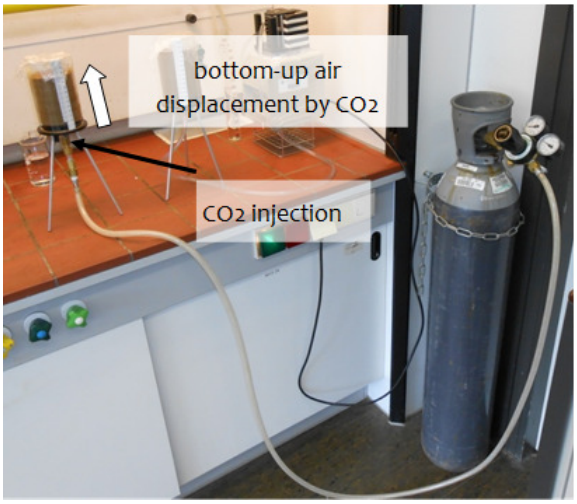

Figure 2.13: Bottom-top low pressure CO_2 injection

Next, water was injected in the columns bottom-up under low pressure, i.e. similarly to CO_2 injection. The water injection rate was 1 ml/sec. As CO_2 is fully miscible in water, the water front advanced in the sand dissolving the gas phase ahead (above) leaving behind it (below) the intended 2-phase system, i.e. water and NAPL. The water saturation procedure is shown in Figure 2.14.

Low pressure injection was applied in both cases in order to avoid firstly entrapment of the displaced gas phase and secondly disturbance of the sand packing which was performed prior to the injections.

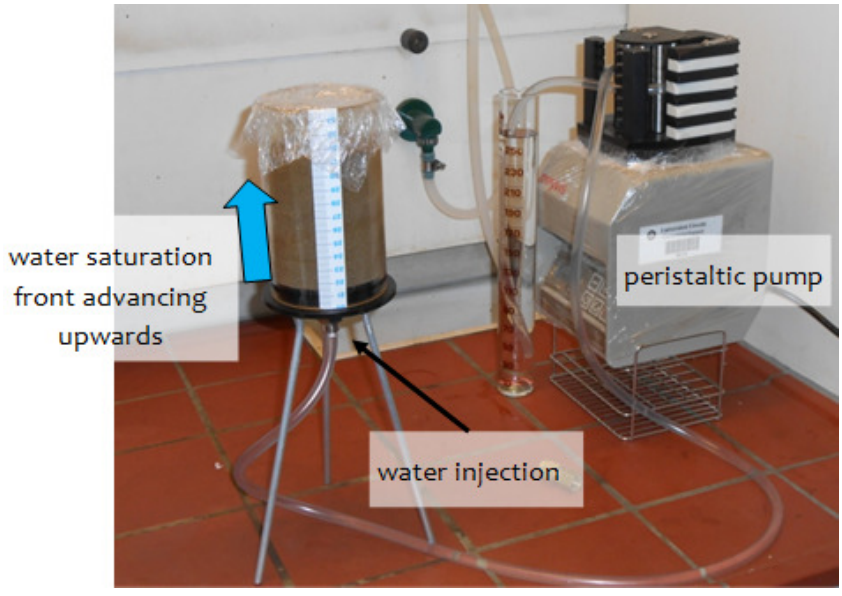

Figure 2.14: Bottom-top low pressure water phase injection

The injected volume of water was measured and together with the measured porosity (see Section 2.2.3.a), were used to calculate the initial total saturation S_{tot}^{i} in the sand.

Note: The above described packing and saturation method was one of the two alternatives examined during the design phase of the experiment. A second method consisting of pouring sand in steps of prescribed weight into a column containing a controlled volume of water and

subsequently disturbing the column by shaking or hitting until the contained sand would match the prescribed height in the column was considered. This method would possibly provide, in comparison with the one implemented, the advantages of unquestionably zero air content and lack of any horizontal layering; however this option was rejected due to the fact that the particular sand carried already an amount of NAPL S^{i}_{NAPL} (see Section 2.1.b) which would blur water in the column resulting a loss of control during the process. Furthermore as already seen in Figure 2.3 horizontal layering is a typical condition encountered at this particular remediation site therefore it was decided not to be excluded from the experiment.

b. Creation of residual NAPL conditions

The aim of the experiments was to evaluate the effect of temperature on the residual/immobile saturation of the NAPL phase. For this reason the saturation of the NAPL phase was brought on its mobility threshold thus able to pick up any effect due to the warming. This mobility threshold is the maximum NAPL residual saturation for these specific circumstances. Two additional experimental phases were designed and executed in order to bring the NAPL saturation at the above described desired level. With the first phase, the NAPL saturation was increased well above the typical mobility thresholds (>>30%). With the second phase the NAPL saturation was adjusted at the maximum residual level (S^{r}_{NAPL}).

This condition was the starting point for warming phase. The initial NAPL saturation (S^{i}_{NAPL}) held already by the sand, although not insignificant, could not be engaged a priori as that threshold saturation level. The reasons were the following:

- As seen in Figure 2.3 the immobile saturation of NAPL was not distributed homogeneously in the sand samples. Parts of the samples carried NAPL saturation while others did not. As both parts of the samples were homogenised for the experimental purposes the macroscopic NAPL saturation dropped due to the homogenisation process.
- The long term in situ dissolution as well as possible further NAPL loss during extraction, sampling and homogenisation had probably lowered the NAPL saturation well below the target mobility threshold.

Increase of NAPL saturation - Drainage

An additional NAPL volume of 36 ml was added in both columns (main and duplicate experiment) by ponding on top of the sand body and drainage. This ponding-drainage process was chosen in order to remain close to the in situ NAPL drainage conditions in the aquifer therefore creating a realistic DNAPL distribution in the columns. In order to minimise boundary effects which would potentially direct a significant fraction of the NAPL amount to drain alongside the hydrophobic column walls (see Section 2.1.a) the ponding and drainage conditions were manipulated. The NAPL volume was drained in the sand driven by a flow boundary condition applied at the bottom boundary of the column. This condition was created by pumping out water from the bottom valve using the peristaltic pump (see Section 2.1.d). In addition, the total amount of NAPL was not ponded at once but in four (4) equal steps of 9 ml. Each of the NAPL mass fractions was completely sucked in the porous medium before the next would take the starting ponded position at the top of the sand. This specific procedure aimed at keeping the ponded NAPL head

on top of the sand low and for a shorter period in place. Moreover it directed drainage towards the vertical axis of the column, i.e. away from the unwanted boundary path at the column walls. At the moment that the total amount of NAPL had entered the sand the flow boundary condition at the bottom boundary of the column ceased. With the total NAPL amount in the sand, the macroscopic NAPL saturation of the system reached the maximum level.

NAPL saturation lowering to SrNW – constant T imbibition cycles

The next step was to decrease the saturation level produced from the previous phase to the maximum residual saturation (S^r_{NAPL}) by displacing all the mobile NAPL towards the outlet of the column (bottom valve). The process was enhanced by pressure driven water imbibition in order to keep the process within a reasonable experimental time scale. The pressure gradient was created between the top and bottom boundaries by ponding water on top of the sand (hydrostatic pressure) and releasing pressure from the bottom valve (atmospheric pressure). The imbibition working together with gravity drainage led the mobile DNAPL to the outflow point of the column leaving behind a distributed trapped/immobilised saturation. Pressure gradient was controlled by adjusting the ponded height of water.

In order to remain close to the in-situ conditions, the first imbibition steps were performed under low pressure. The aim was to allow the migrating NAPL phase to drain along naturally chosen pathways. Once the initial spreading of the NAPL in the columns was assumed complete the system was switched to the high pressure condition.

As a first low pressure step a height of 2cm ponded water (corresponding pressure P_w^i=0.2 kPa[3]), was applied on top of the sand. This pressure was not kept constant but it was let drop to zero as mass flew out of the bottom valve (P_w^{drop}=0.2 kPa). Next, a second similar low pressure step of 4cm ponded height (P_w^i=0.4 kPa) was applied. During that step, the pressure was once more not kept constant but it was let drop to 2cm (P_w^f=0.2 kPa, P_w^{drop}=0.2 kPa). After the second low pressure step, the pressure at the top of the sand was increased at the maximum of 5 kPa, i.e. 50 cm height of ponded water. This pressure boundary condition at the top boundary was thereafter applied in combination with the atmospheric pressure at the bottom boundary to drive the flow through the porous medium during all the later phases of the experiment. The pressure was sustained using the peristaltic pump to pump water from a reservoir to the pressure tube of the column maintaining the height of ponded water at the aforementioned level (see Figure 2.15).

During the beginning of the imbibition phase, the first difference between the main and duplicate experiments was applied. In column 2 (duplicate experiment) the second low pressure step was skipped taking the system directly to the high pressure condition.

Flow condition was not applied constantly but periodically. The top boundary condition, i.e. water pressure, was kept constant but the bottom boundary condition was alternated between the no flow condition (boundary closed) and the atmospheric pressure condition (boundary open-flow condition). The flow condition functioning as production step was maintained to collect 2 pore volumes of liquid product from the outflow (bottom) valve. It was then switched to the non-flow

[3] Water pressure calculated on the base 10 kPa per m of water height

condition. The non-flow interval between two consecutive production steps was approximately 1 hour.

From the beginning of this phase all the outflow of liquids was collected in sample H.D.P.E. bottles. The amount of product was measured in pore volumes (hereafter also mentioned as P.V.). The particular phase of the experiment ceased at the point that NAPL production reached a constant low equilibrium level. At that point the macroscopic NAPL saturation (S^r_{NAPL}) was considered irreducible and therefore the system met the requirement for the limited warming to be applied.

The NAPL saturation lowering phase was split into two steps. During the first step the main bulk of imbibition cycles were performed amounting a total of 38 P.V. per column experiment. With this step the largest part of mobile NAPL saturation was removed from the columns and NAPL production was stabilised at a significantly low level indicating that the NAPL phase remaining in the columns was practically immobile. The evaluation of the NAPL production was based on optical observation of the mixed product. The second step consisting of 8 P.V. per column experiment and aimed at verifying the equilibrium saturation conditions. The interval between the two steps was 24 hours for column 1 and 72 hours for column 2 and intended at allowing any time related gravity drainage of remaining mobile NAPL to evolve, i.e. within the specific experimental time scale, before NAPL saturation was regarded as residual. Since the 24 hours held for Column 1 might have been insufficient, the interval time was tripled for Column 2.

The pressure and head diagrams of the three steps are given in the Appendix I. For column 2 only steps 1 and high pressure step apply.

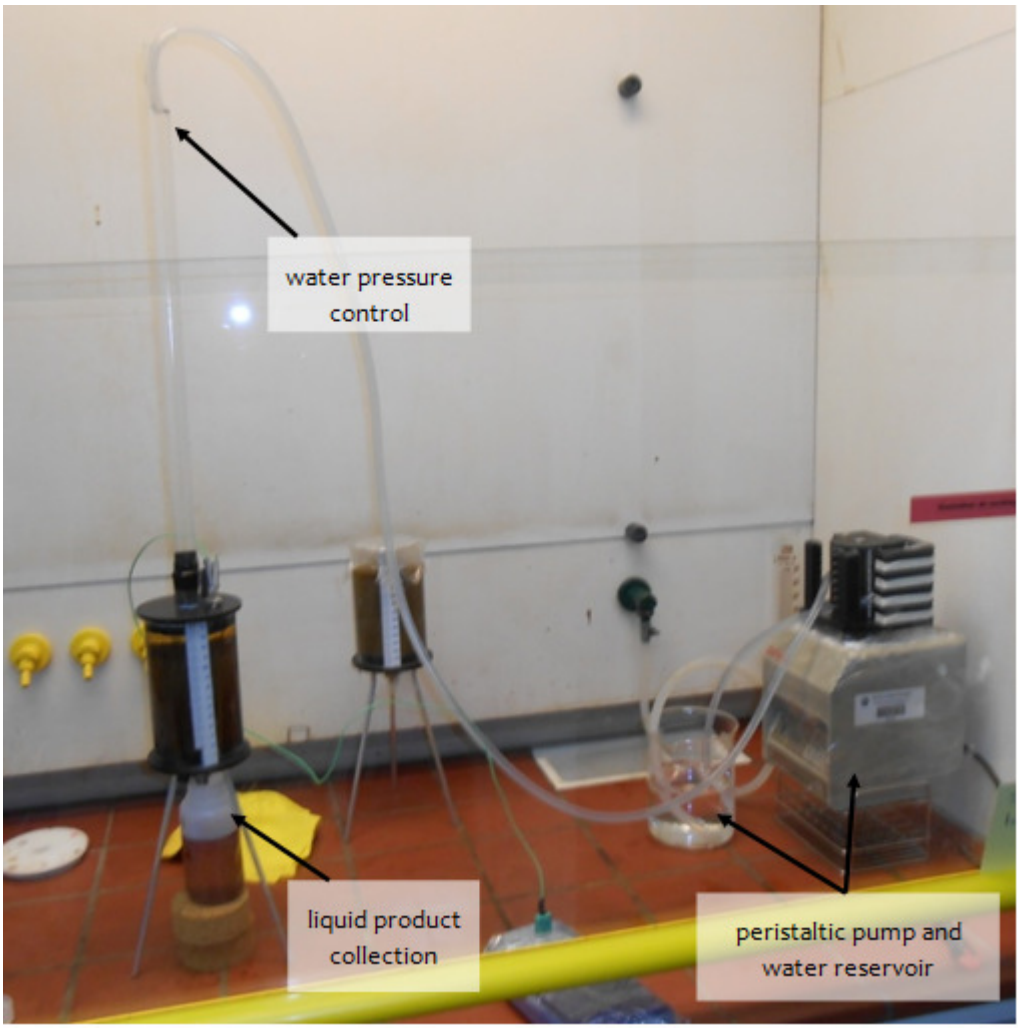

Figure 2.15: High pressure imbibition procedure

c. *Temperature variation phase; warming and cooling phases*

The 2-phase system produced from the previous phases with the NAPL saturation at S^{r}_{NAPL} was the starting point for the temperature variation phase. Until that point temperature was kept constant at 21°C (standard laboratory ambient temperature). From that point it became the only variable parameter[4] of the system in order to assess its effect on macroscopic NAPL saturation. The effect of temperature was quantified from the variation of NAPL production. In order to fully assess the effect of temperature variation three consecutive experimental sub-phases were carried out:

1. Limited warming at 50°C
2. Restoration of temperature at the base level of 21°C
3. Cooling at 12°C

In this way, apart from the limited warming effect, the response of the system to the restoration of temperature at the initial conditions (21 °C) and subsequently to cooling (12 °C) was assessed.

[4] Pressure was kept constant at the maximum level, i.e. 5 kPa at the top of the sand

Especially for the cooling phase, the aim was to reverse the temperature conditions and together the initially applied gravity-interfacial tension perturbation in order to evaluate the corresponding effects on NAPL production and to gain overall insight on the effect of temperature variation.

Temperature conditions of the porous medium and liquid phases were altered using the warm water bath and silicon tubing (see 2.1.d). The peristaltic pump (part of the warm water bath) was used to circulate water at a set temperature from the warm water bath, through the silicon tubing and back to the water bath. As the silicon tubing was wrapped around and in contact with the walls of the column, heat was conducted from the tubing to the column walls and finally to the interior of the column. In order to reduce temperature losses insulating aluminium sheet was wrapped around the silicon tubing (see Figure 2.17). This process gradually altered the temperature of the porous medium and contained liquids until the uniform constant target level. Heat was conducted inwards during warming and outwards during cooling. Temperature was monitored at the two boundaries of the system, i.e. the warm-water bath and the interior of the column. The latter was done using the thermocouples-data logger system (see 2.1.d). In this way the heat loss between the warm water bath and the interior of the column was quantified and compensated accordingly. Sand, water and NAPL in the column were assumed to be under the same temperature level, that of the thermocouple output. The procedure is given in Figure 2.16.

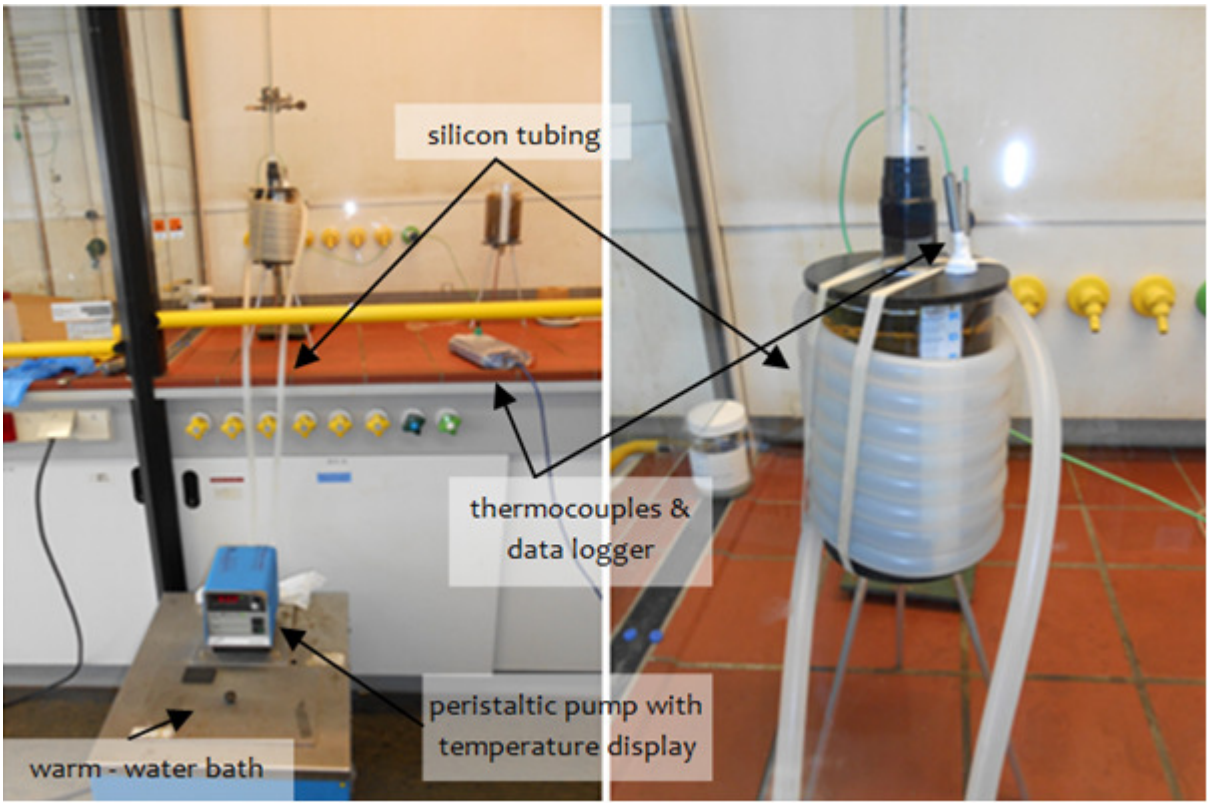

Figure 2.16: Warming/cooling procedure

During the warming phase, the temperature in the column was raised to 50°C. As soon as the monitored temperature in the columns settled at the intended level, the production restarted by the circulation of water, following the same method as described in Section Creation of residual NAPL conditions2.2.2b. The top boundary condition was kept constant at the maximum pressure, i.e. 5 kPa, while at the bottom boundary the condition was alternated between the flow and non-

flow condition. During this phase the temperature of circulated water was set at 50°C. This was achieved by warming water in a reservoir using the warming plate (see Figure 2.6.c) and controlling its temperature with an extra thermocouple in that reservoir. The peristaltic pump was used to pump water from the reservoir to the pressure tube of the column. The procedure is given in Figure 2.17 below.

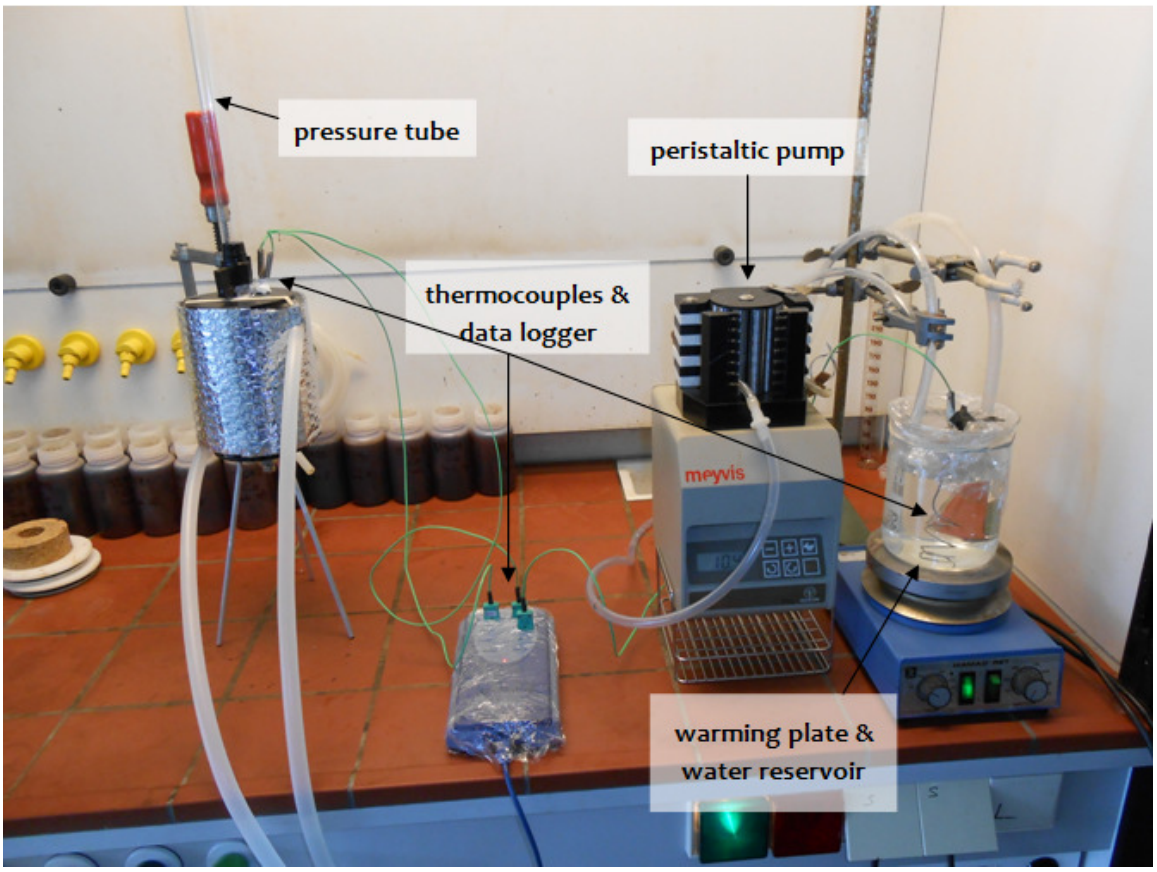

Figure 2.17: Water circulation during warming/cooling phases

During both reversing and cooling phases the system was first left to equilibrate at the new conditions and then production cycles restarted with the circulation of water at the same temperature as that of the interior of the column, i.e. similarly to the warming phase. In the case of cooling, water in the reservoir was cooled using ice.

During these temperature related phases the second difference in the experimental procedure between the main and duplicate experiments was applied. This was the number of pore volumes circulated and the total duration of the warming and restored temperature phases. For the cooling phase procedure was identical. The number of pore volumes circulated per temperature phase is given in Table 2-2. The duration of the experimental phases for the two experiments are given in Figure 2.18.

phase	P.V. C1	P.V. C2
T ct at 50°C	14	8
T ct at 21°C (restored)	12	8
T ct at 12°C	12	12

Table 2-2: Pore volumes of water circulated for the two experiments (C1 & C2)

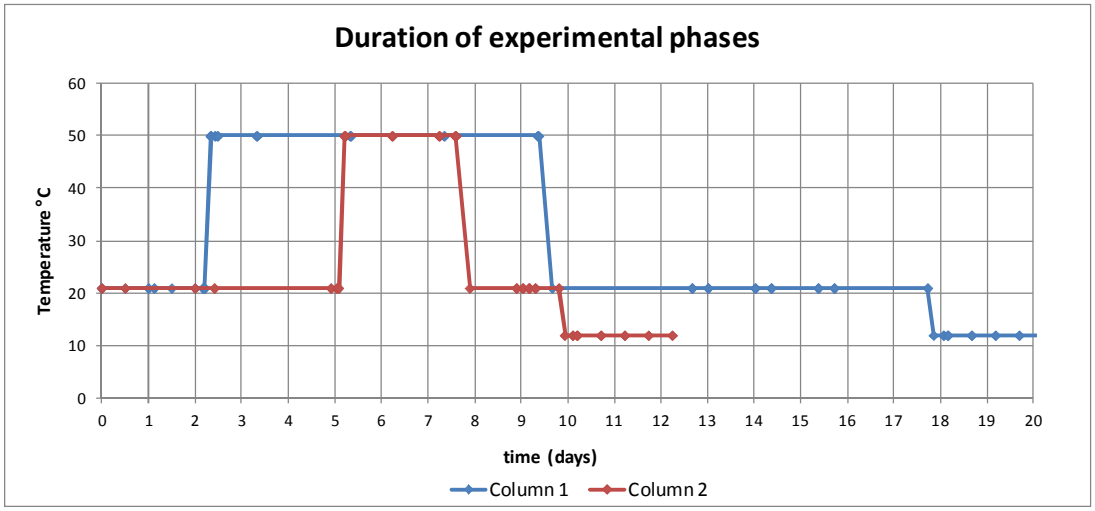

Figure 2.18: Duration of experimental phase for the two experiments

2.2.3. *Measurements*

In this section the measurements methods related to the column experiment are presented. The target was to determine the saturation of the NAPL in the columns both as an absolute number at the end of the experiment as well as the change of saturation during the experimental phases. The nature the two main materials used, i.e. sand and NAPL, created the need for application of non-conventional measurement methods. These methods were engineered and calibrated in order to suit those two materials. In particular, the following characteristics of the two materials functioned as complicating factors. These factors either restricted the range of applicable measurement methods or required an independent and multistage measurement procedure.

- The sand was used in the experiment as collected from field carrying an unknown mixed initial saturation of both water and NAPL phases.
- The density difference between this NAPL and water is approximately 3%. Therefore all the direct gravimetric measurements, i.e. weighing a known volume of mixed product and determining the two fractions on the basis of the phase densities, were within the error margin.
- The particular NAPL type (oil-gas tar) is extremely adhesive, even on normally hydrophilic surfaces like glass. This resulted in mass loss during every mass transfer of NAPL. Therefore no transfer of the experimental product (mixed NAPL and water phases) from the sample bottles to other vessels was performed.
- The product of the experiment was an emulsion of NAPL and water phases requiring the application of a separation method.

a. *Sand cleaning – Porosity – Initial total saturation*

Packing in the column and subsequent saturation (Section2.2.2a) were carried out with the sand containing the mixed initial saturation S_{tot}^{i}. For this reason, porosity could not be measured

directly, i.e. volumetrically during saturation. Instead a completely independent and combined procedure was followed in order to measure porosity for the particular packing of sand in the columns, and initial total saturation S_{tot}^{i}. Further, the two fractions of S_{tot}^{i}, S_{water}^{i} and S_{NAPL}^{i} of each of the two liquid phases respectively, was determined based on a second and also independent procedure, presented in Section 2.2.3b.

As porosity depends on packing density, the reference point for the procedure was the density of sand packed in the columns at its initial state, i.e. containing the mixed S_{tot}^{i}. This, as analysed in Section 2.2.2a, corresponded to a common value of unsaturated sand unit weight, i.e. 18 kN/m^3, which translated in terms of mass and experimental scale corresponds to 1.8 g/cm^3 (ρ_{sand}^{i}). In order to determine porosity, the mass of sand corresponding to a unit volume for the particular sand packing, was first taken to zero saturation providing the W_{sand}^{dry} per unit volume. Subsequently the NAPL free and dry sand was packed at the unit volume and was fully saturated with water providing the W_{sand}^{sat} per unit volume. Porosity was calculated volumetrically, from the volume of water added to reach the fully saturated condition per sand unit volume, and gravimetrically using the following formula:

$$n = \frac{W_{sand}^{sat} - W_{sand}^{dry}}{\rho_{water}} * \frac{1}{V_{ref}}$$

where: n is the calculated porosity and V_{ref} the reference or unit volume

Taking sand to a completely dry state required two different steps. First sand was flushed with the most effective of the tested organic solvents for the particular NAPL type, Acetone (C_3H_6O), in order to remove the persistent S_{NAPL}^{i}. For this purpose, a known weight of initial sand W_{sand}^{i} was placed on an inertial filter bound on a laboratory vessel in order to allow flushing with Acetone. In this way the dissolved NAPL was carried through the filter slots in the vessel below. Procedure and result of sand cleaning are given in Figure 2.19.

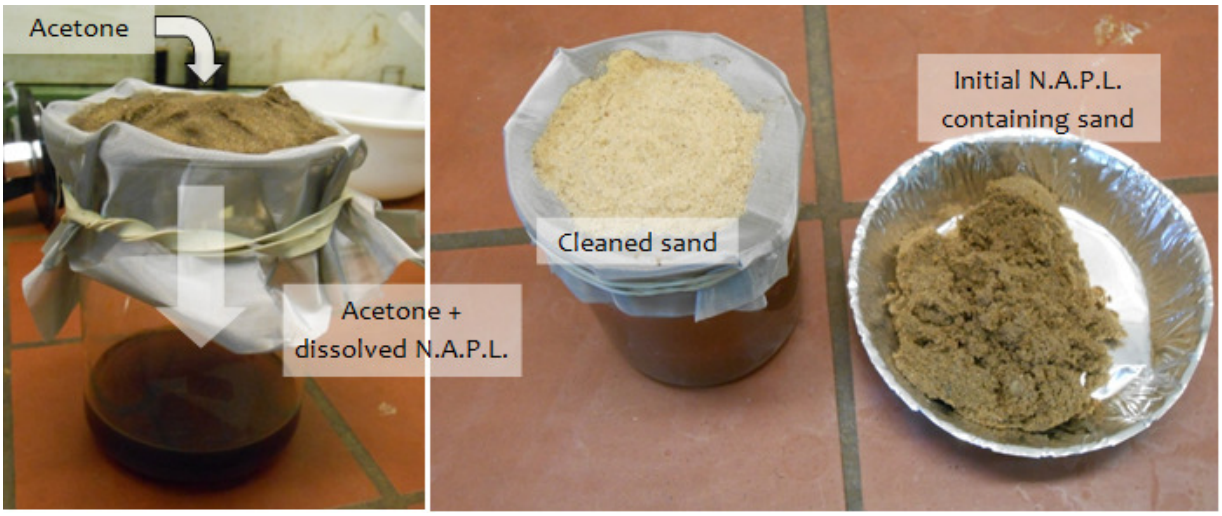

Figure 2.19: Sand cleaning procedure and result

Subsequently, the cleaned sand was dried in oven at 100 °C for 3 hours for the intended NAPL free and dry sand to be produced.

With known W_{sand}^{dry} the initial mixed saturation of the sand S_{tot}^{i} could be calculated by the difference between W_{sand}^{i} and W_{sand}^{dry} for the same unit volume. Given the already calculated porosity and assuming that the average $\rho^{liquids}$ is equal to 1 g/cm^3, S_{tot}^{i} was calculated using the following formula:

$$S_{tot}^{i} = \frac{W_{sand}^{i} - W_{sand}^{dry}}{\rho^{liquids}} * \frac{1}{n}$$

b. Evaporation rates - NAPL saturation

Evaporation rates

The difference in the evaporation rates of the two liquids, i.e. NAPL and water, was quantified in order to serve as the phase separation method. This method was applied in the following two types of measurements.

- Separation of the NAPL from water from hydrophilic filters in order to measure the free NAPL product of the column experiment
- Separation of the NAPL from water from sand in order to estimate the initial NAPL saturation S_{NAPL}^{i}

Initially, the rate of evaporation of the NAPL from the free top surface of the liquid phase in a laboratory vessel in the laboratory fume-hood was measured. This measurement was carried out at two temperatures: 21°C and 50°C. The results are given in Figure 2.20 below.

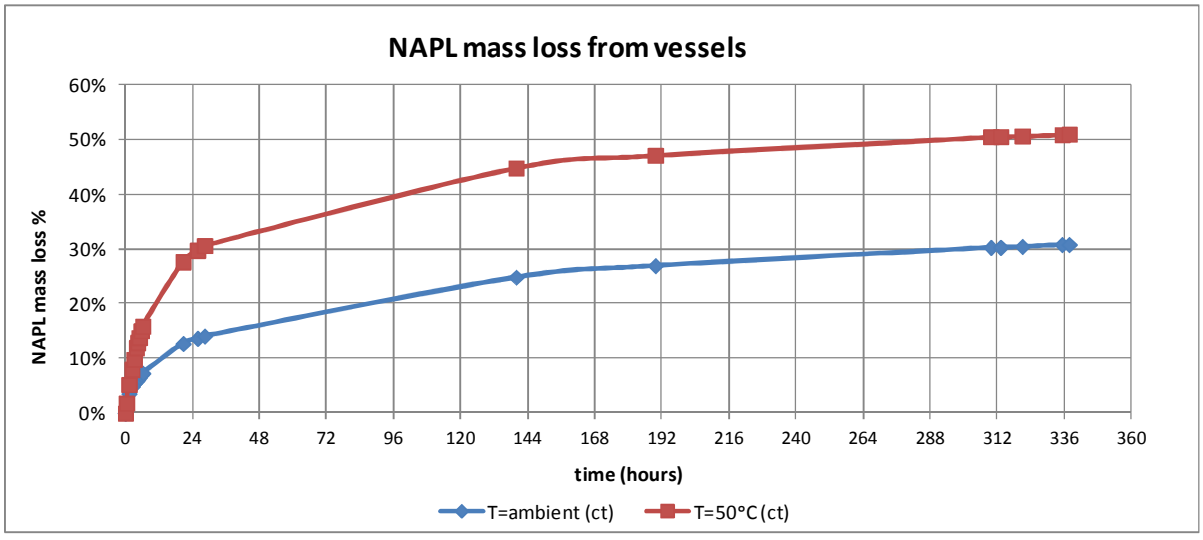

Figure 2.20: Evaporation rate of the NAPL from a free surface in vessel in the fume hood

The conclusion was that NAPL evaporation rate is clearly ordered by its multi-component composition (see Table 2-1). During the first period of exposure, when the most volatile

components evaporate, the rate of evaporation is high. Gradually, as the most volatile components are depleted, the evaporation rate drops finally approaching practically zero, i.e. for the particular time scale. The total NAPL mass loss hardly exceeded 30% and 50% for 21°C and 50°C respectively. This result indicated that a considerable fraction of the NAPL components is insignificantly volatile for the particular time scale.

Evaporation rate depends heavily on the free surface of the liquid phase, which in turn depends on the configuration of each system in particular. As the separation method based on the difference of evaporation rate would be applied on two different systems, the evaporation rates of the NAPL and water were quantified while occurring from the pore space of two different types of porous medium.

The first porous medium type tested was the hydrophilic filters. The hydrophilic filters were used for NAPL-water separation from the mixed condition (emulsion) of the liquid product of the column experiment (see Figure 2.23). Different tests were performed in order to determine the rate of evaporation from the filter of each liquid alone. For the water test pieces of hydrophilic filter of known weight were initially soaked in water, thereby capturing full water saturation. Subsequently they were placed in the fume-hood for the evaporation process to start. The filters were weighed at regular time intervals until all the containing water evaporated and the filters returned to their initial dry weight. For the NAPL test specific amount of free phase NAPL (1, 2 and 3 ml) was poured on the hydrophilic filters of known weight. The NAPL containing filters were subsequently placed in the fume hood. Filters were weighed at regular time intervals. This time they did not return to their initial weight because, as expected based on the findings of NAPL evaporation test from vessels (see Figure 2.20), only a fraction of the NAPL mass was lost due to evaporation. The results are given in Figure 2.21, below.

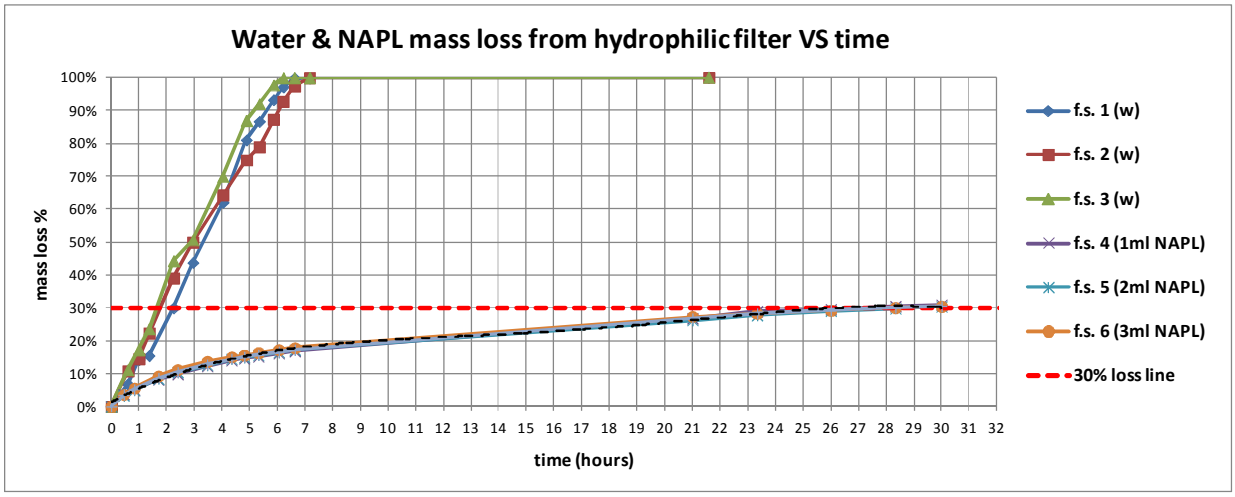

Figure 2.21: Evaporation rate of water and NAPL from hydrophilic filter in the fume hood (f.s.: filter sample)

Results indicated the following:

- the whole water amount could evaporate, allowing the filter to return to its initial dry weight after approximately 3 hours
- NAPL evaporation, similarly with the vessel test described above, initially occurred at a high rate. The rate dropped with time approaching practically zero after approximately 24

hours. The equilibrium mass loss at that point amounted 30% of the initial NAPL mass in all three cases.

The second type of porous medium tested was the NAPL free (cleaned) dry unpacked sand (see Figure 2.19). This system found application later on the estimation of the initial NAPL saturation S^i_{NAPL} held in the field samples. Once more, as in the case of the hydrophilic filters test, two different tests were performed in order to determine the rate of evaporation of NAPL and water from the dry clean sand. These tests were performed in an identical manner; the same mass of dry cleaned sand (1.65 g) was placed unpacked on two laboratory aluminium plates and sand was oversaturated with the same excessive volume (0.8 ml) of different liquid for each case (NAPL/water). Subsequently, the two plates were left in the fume-hood and regular weight measurements were performed as evaporation of liquids proceeded. The results are given in Figure 2.22 below.

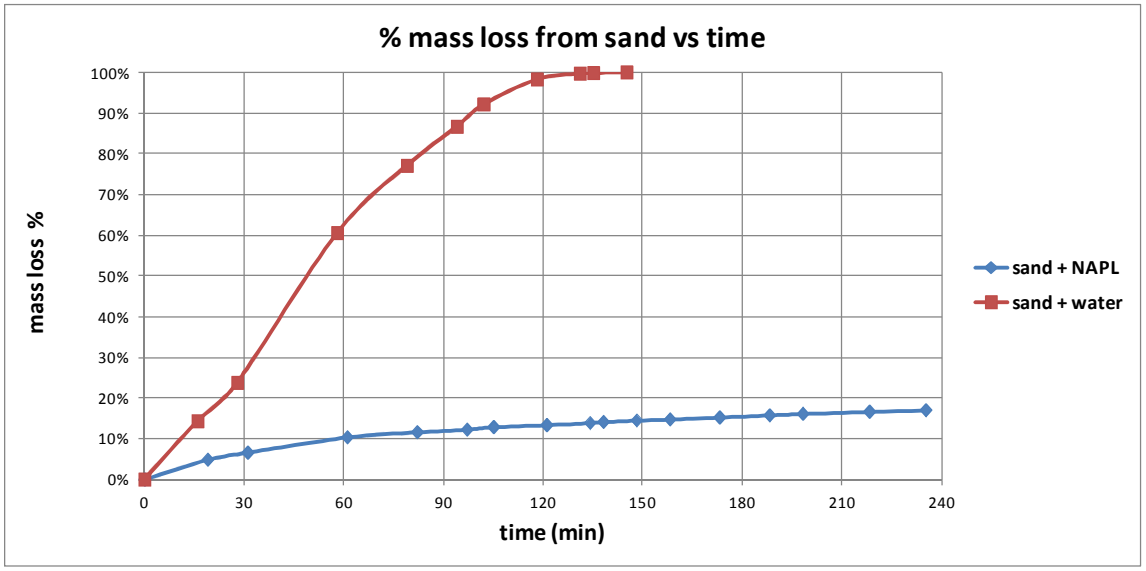

Figure 2.22: Evaporation rate of water and NAPL from sand

Results for the particular porous medium indicated a similar behaviour as in the case of the hydrophilic filter test. Water mass could fully evaporate within a particular interval of time (approximately 2 hours for this case) and NAPL rate of evaporation is significantly lower.

NAPL saturation

Saturation in the columns was quantified based on the measurements of pure phase NAPL produced during the different phases of the experiment. The change of macroscopic saturation was quantified by subtracting the NAPL amount contained in every pore volume of mixed product (water and NAPL) from the maximum saturation of NAPL at the end of the drainage phase. The maximum NAPL saturation amounted the sum of the initial NAPL saturation in the sand (S^i_{NAPL}) plus the additional drained NAPL volume over the total pore volume. It was therefore necessary to quantify both the free NAPL produced and the initial NAPL saturation. The relevant equations are given below:

$$S_{NAPL}^{\max} = S_{NAPL}^{ini} + S_{NAPL}^{added}$$

$$S_{NAPL}^{end} = S_{NAPL}^{\max} - dS_{NAPL}^{prod}$$

NAPL product measurement

For the measurement of NAPL mass which was part of the mixed product the following series of actions was carried out. The mixed product of the experiment was collected in standard HDPE bottles (see Figure 2.15). This complicated the measurements as the organic HDPE material adsorbed a fraction of the already low (compared to water) NAPL amount contained in each of the bottles. This required the NAPL product measurements to be split in two separate measurements, this of the free NAPL mass in the mixed liquid phase and that of the adsorbed mass on the HDPE bottles. The two amounts were summed up to provide the intended result.

For the measurement of the free NAPL mass in the mixed liquid product the two liquid phases, i.e. water and NAPL, were separated using hydrophilic filters. The mixed liquid product was poured on the top of the filter, which given its hydrophilic character, allowed only the water phase to flow through its pores and break through. The NAPL phase either ponded on top of the filter or was captured in the pores. The procedure is given in Figure 2.23.

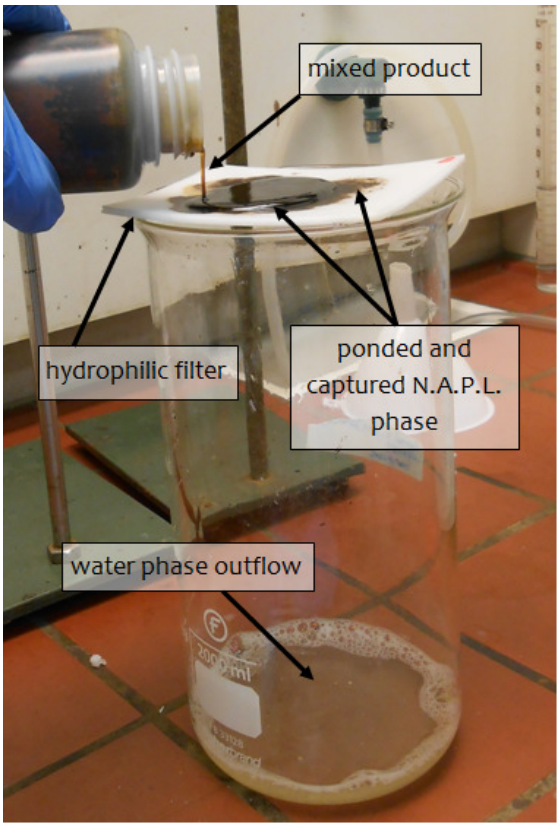

Figure 2.23: Phase separation using hydrophilic filter

With this procedure most of the water phase was separated from the mixture, however a small fraction remained entrapped in the pores of the filter together with the NAPL phase. In order to measure only the NAPL mass, the remaining water phase was completely eliminated from the filter with a second separation step. For this second step the difference in evaporation rate of the

two phases from the pores of the hydrophilic filter was put to use. The filters carrying both water and NAPL were placed in the fume hood and were left for 24 hours. This time period was chosen in order firstly to make sure that the entire amount of water would evaporate from the filter and secondly to allow the 30% mass loss to be used for the correction of the NAPL mass due to evaporation (see Figure 2.21). The NAPL mass was calculated by the difference of initial (dry-before use) and final filter weight applying the aforementioned 30% correction. This provided the free NAPL mass component of the product.

For the measurement of the NAPL mass adsorbed on the surface of the H.D.P.E. sample bottles, after the entire free mixed product was removed, the hydrophobic bottles were left to drain from the water phase, holding eventually only the adsorbed NAPL mass. By the difference of initial (before use) and final bottle weight the adsorbed NAPL mass component of the product was quantified.

Finally, the sum of the two measurements provided the NAPL mass produced per pore volume of mixed product.

The described sequence of actions, i.e. measurement of free and adsorbed NAPL mass, was first tested as a complete sequence to measure the NAPL mass contained in mixed liquid test samples. These tests concluded an error lower than 3%, which allowed the application of the method to the actual NAPL mass measurements.

The relevant equations are given below:

$$W_{NAPL}^{free} = (W_{filter}^{24h} - W_{filter}^{ini}) * (\frac{100}{100-30}\%)$$

$$W_{NAPL}^{ads} = W_{bottle}^{end} - W_{bottle}^{ini}$$

$$W_{NAPL}^{tot} = W_{NAPL}^{free} + W_{NAPL}^{ads}$$

$$dS_{NAPL}^{prod} = \frac{W_{NAPL}^{tot} / \rho_{NAPL}}{PV^{column}}$$

NAPL initial saturation estimation

The initial saturation of NAPL S_{NAPL}^{i} held by the sand (see Figure 2.3) was estimated using the difference in evaporation rates of the two liquid phases, i.e. water and NAPL. The method was based on the findings of the tests quantifying the evaporation rates of the two liquids from the pores of unpacked sand (see Figure 2.22). According to the results of these tests the entire water mass evaporates from the sand pores within a specific period while NAPL evaporation evolves at considerably lower rate. This difference allowed the indirect quantification of the liquid masses present. The procedure was similar to the one followed for the measurement of the mobile NAPL product of the column experiment based on the difference of evaporation rates of the two liquids from the pores of the hydrophilic filter. However a major difference applied between the two cases.

In the case of the mobile product the calibration of the method was complete as the mobile product produced from the column experiment was considered to have retained its initial composition (see Table 2-1). It was therefore possible to quantify the evaporation rate of the free NAPL product by running parallel tests. Furthermore it was possible to test the entire procedure using test samples of mixed phases and conclude on its accuracy and applicability. On the contrary, the NAPL mass carried in the sand pores at the in situ state could not be considered identical with the free phase NAPL. The residual phase NAPL had remained in-situ, trapped and discontinuous in the sand pores, surrounded by water phase for a very long period of time, possibly longer than 50 years (see Section 1.2). It was therefore logical to assume that the composition of this NAPL residual phase differs from the initial composition of the free NAPL phase due to dissolution of components in the surrounding water phase. In addition, sand samples were exposed to atmospheric conditions during both extraction from the boreholes and homogenisation before laboratory use allowing the volatile components to evaporate. Hence the evaporation rate of this NAPL saturation was expected to differ from the evaporation rate of the free phase NAPL as this was quantified during this experimental study (see Figure 2.22).

Since it was impossible to extract residual NAPL phase from the sand and define its own properties, it was assumed that the evaporation rate was bound between a minimum and a maximum. The minimum rate was taken as zero, assuming that the NAPL carried in the sand contained no volatile components. The maximum was taken equal to the evaporation rate of the free phase NAPL for specific time interval of exposure based on Figure 2.22. The free phase NAPL was assumed to contain the maximum fraction of volatile components producing thereby the highest evaporation rates thus the maximum NAPL mass loss.

The second limitation of this method was the fact that the density of the residual phase was unknown and non-quantifiable. Because of that for the conversion of weight to saturation a reference density was used taken equal to the density of free NAPL phase at ambient temperature ρ_{NAPL}^{ref} as this was defined during different phase of the experimental procedure, i.e. 1.03 g/cm^3 (see Section 2.2b).

The applied method for the estimation of the S_{NAPL}^{i} consisted of the following steps:

- Known weight of initial sand W_{sand}^{ini}, i.e. sand carrying both NAPL and water, was placed unpacked in aluminium laboratory vessel. This weight corresponded to a reference volume V_{sand}^{ref} according to the packing unit weight of initial sand in the columns (1.8g/cm^3).
- The weight of the laboratory vessel W_{ves}, was known. The total weight of the vessel with the containing sand is

  $$W_{total}^{ini} = W_{ves} + W_{sand}^{ini} \quad (1)$$

- The weight of initial sand corresponded to a weight of NAPL free dry sand (W_{sand}^{dry}) as already defined in different phase of the experimental procedure (see Section 3.3.a). The initial weight of liquids in the sand was calculated from:

$$W_{liquids}^{ini} = W_{sand}^{ini} - W_{sand}^{dry} \quad (2)$$

- The vessel was placed in the fume hood for evaporation of both liquid phases to evolve
- Total weight was measured at regular time intervals W_{total}^{i} and the lost weight of liquids was calculated from:

$$W_{liquids}^{lost} = W_{total}^{ini} - W_{total}^{i} \quad (3)$$

- $W_{liquids}^{lost}$ was put in diagrams with time.
- The time point when the entire mass of water had evaporated was defined from the curves based on the change of evaporation rate as seen in Figure 3.7 in correspondence to Figure 2.22
- The liquid mass remaining in the sand, assuming no water was present was calculated from:

$$W_{rem}^{n} = W_{liquids}^{ini} - W_{liquids}^{lost} \quad (4)$$

- Water was assumed to have evaporated fully, hence:

$$W_{rem}^{n} = W_{rem}^{NAPL} \quad (5)$$

- NAPL mass loss due to evaporation was considered to be bound between a maximum and minimum. The NAPL loss is expressed in terms of percentage $m\%$ of the initial NAPL mass. The average NAPL mass loss percentage was:

$$m^{avg} = aver(m^{\min}; m^{max}) \quad (6)$$

- The total NAPL mass initially in the sand was calculated from the formula:

$$W_{NAPL}^{ini} = \frac{W_{NAPL}^{rem}}{(1 - m_{NAPL}^{avg})} \quad (7)$$

- The reference density of sand Volume of NAPL initially contained in the sand was calculated from:

$$V_{NAPL}^{ini} = \frac{W_{NAPL}^{ini}}{\rho_{NAPL}^{ref}} \quad (8)$$

- Initial saturation of the NAPL in sand was calculated from:

$$S_{NAPL}^{ini} = \frac{V_{NAPL}^{ini}}{n * V_{sand}^{ref}} \quad (9)$$

- The test was repeated for different weight of initial sand.
- The test was repeated with additional mass of water added to the unpacked initial sand; this water was added in a way that it flushed the unpacked sand in order to disrupt water

phase entrapment between the sand grains and NAPL coatings. In this case the $W_{liquids}^{ini}$ was calculated from:

$$W_{liquids}^{ini} = W_{sand}^{ini} - W_{sand}^{dry} + W_{water}^{+} \quad (2^*)$$

c. Flow rates

The drainage process was performed with a known flow rate (flow driven drainage). The flow rates of the wetting phase during the imbibition and the temperature variation phases were not measured. The flow rate of the wetting phase was measured at the end of the experiment, when the NAPL saturation had reached the minimum level, thus the relative permeability and corresponding flow rate of the wetting phase was maximised (q_w^{max}). The wetting phase flow rates during the temperature variation phases were back-calculated applying Darcy law for different viscosity values (see Figure 2.5), as it was assumed that the flow wetting phase relative permeability remains practically unchanged for a non-wetting phase already at residual saturation. For the constant T imbibition phase, at which the non-wetting phase saturation was changing the above back - calculation was not possible; for this phases the wetting phase flow rate could only be assumed lower than the end-measured maximum flow rate (q_w^{max}). Based on those flow rates the Capillary numbers were calculated based on the formula:

$N_{ca} = \frac{q\mu}{\gamma \cos\theta}$ [7], where q: Darcy velocity [L/T], μ: viscosity of the displacing fluid [FT/L^2], γ: interfacial tension [F/L] and θ: contact angle [7]

3. RESULTS

3.1. Wettability

The result of the wettability test is shown in Figure 3.1.

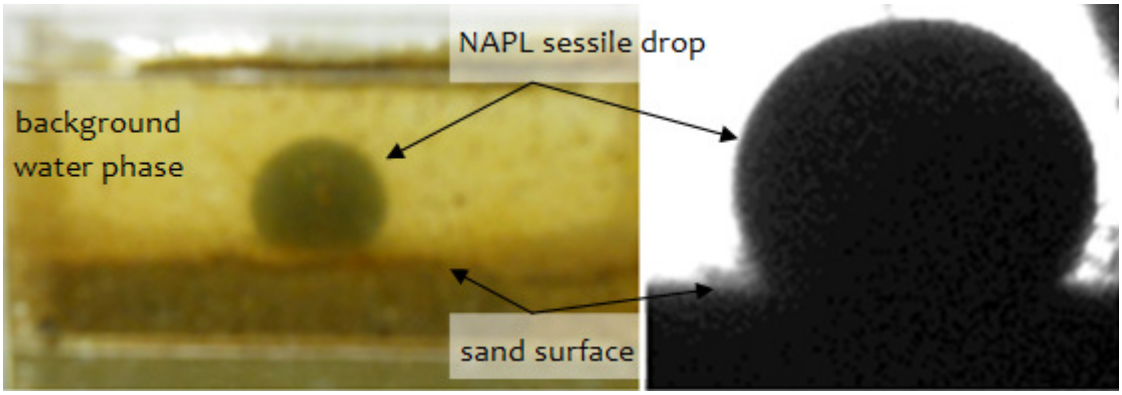

Figure 3.1: Sessile drop wettability test results

The contact angle at the intersection of the sand surface with the two liquid phases is clearly below 90°-ψ[5]. Based on this result the porous medium was verified as water wet. Additional photographic profiles of sessile drops are given in Appendix III.

3.2. Gravity & Interfacial tension

3.2.1. Gravity

The results of the NAPL density measurements at different temperatures are shown in Figure 3.2.

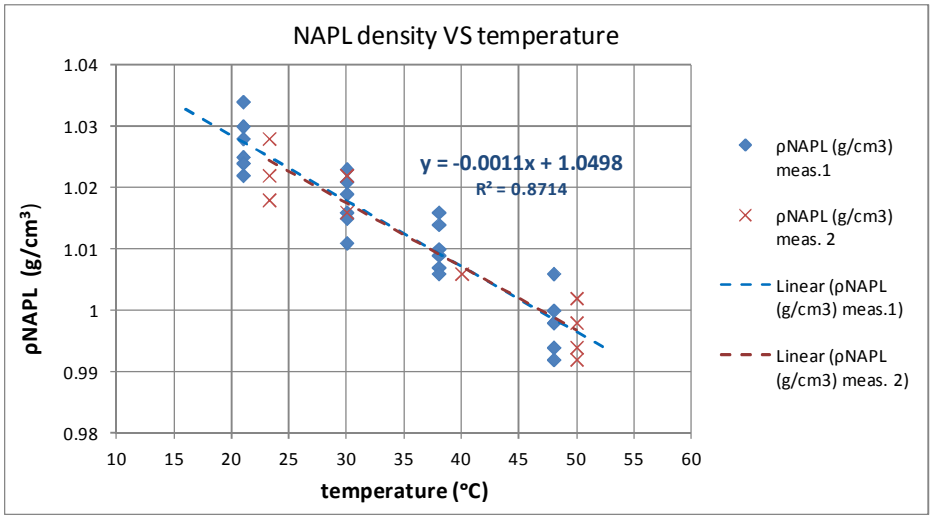

Figure 3.2: NAPL density vs temperature

The NAPL density is dropping with increasing temperature, even below 1 g/cm^3 for temperature higher than 45°C. The results were integrated in the following $\rho_{NAPL} = f(T)$ equation:

[5] ψ: tolerance level of 20° [1]

$$\rho_{NAPL}(g/cm^3) = -0.0010664 * T(°C) + 1.0497733$$

In combination with the respective $\rho_{water} = f(T)$ given in Section 2.1.c the density variation with temperature of the two experimental phases, i.e. NAPL and water, for the range of 15 to 50°C is given in Figure 3.3.

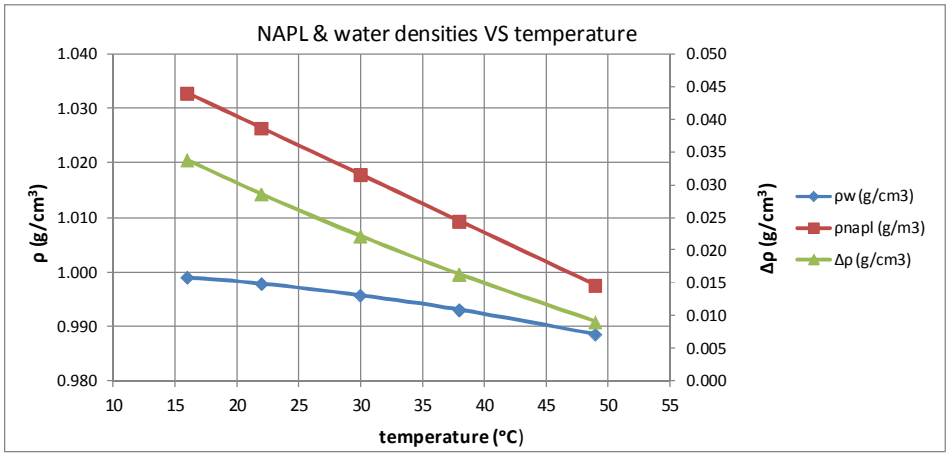

Figure 3.3: Comparison NAPL and water densities vs temperature

The density of the NAPL decreases more compared to water, resulting in decreasing density difference with increasing temperature for the particular temperature range. The density difference of 0.035 g/cm³ at 15°C drops below 0.01 g/cm³ at 50°C.

3.2.2. *Interfacial tension*

The variation of the dimensions of pendant drops with temperature within the range of 15 to 51°C expressed by the radius of curvature at the drop apex and the diameter ratio is shown in Figure 3.4.

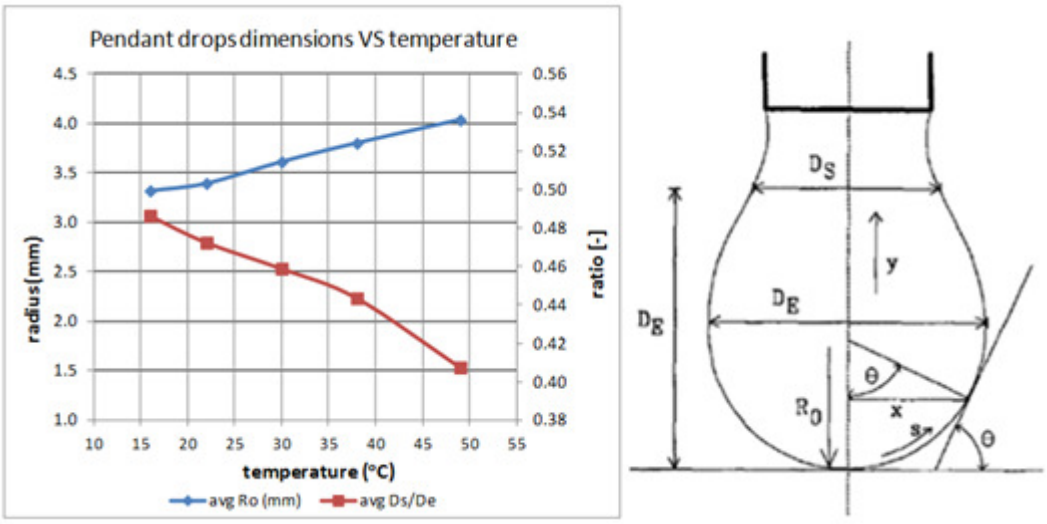

Figure 3.4: Pendant drop dimensions vs temperature

The results indicate that the size of pendant drops of NAPL in water phase increases with increasing temperature. Photographic profiles of pendant drops at different temperatures aer given in Appendix II.

Using the dimensions of the pendant drops and the density difference of the two phases the interfacial tension for the particular temperature range was calculated as discussed in Section 2.2.1c. The results are shown in Figure 3.5 as compared to the density difference variation with temperature.

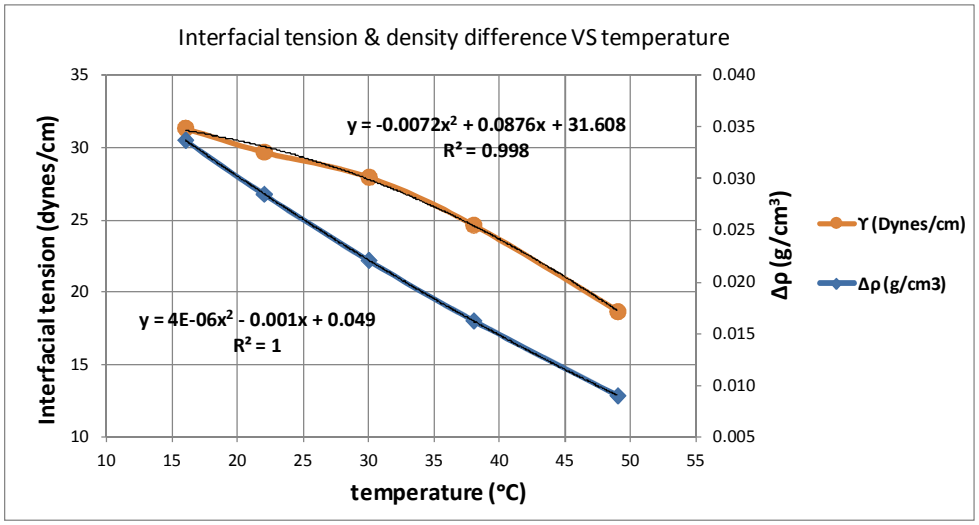

Figure 3.5: Interfacial tension and density difference vs temperature

The interfacial tension of the two liquids decreases with increasing temperature. From a value of approximately 32 dynes/cm at 15°C it drops to less than 18 dynes/cm at 50°C. The drop of interfacial temperature and density difference of the two liquids expressed as percentage from the values at 15°C is given in Figure 3.6.

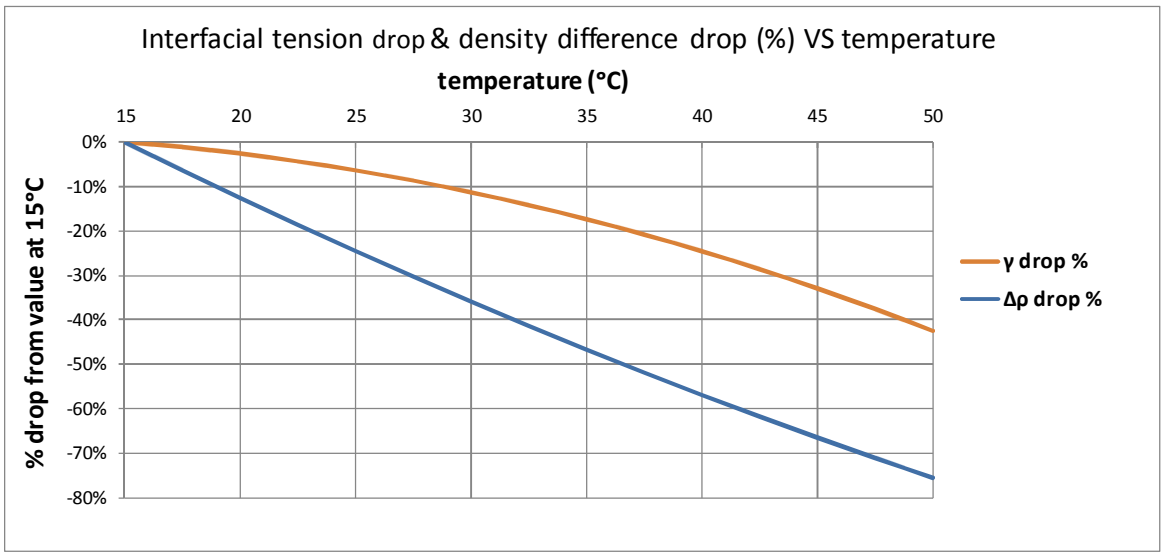

Figure 3.6: Comparison of drop of interfacial tension vs drop of density difference with increasing temperature

Based on the results, the increase of temperature from 15 to 50°C, results in a 40% drop of interfacial tension and an almost double (76%) drop of density difference. In terms of vertical equilibrium with increasing temperature[6] the decreased interfacial tension is opposed to a more decreased gravitational force. This fact reasons the increasing size of pendant drops with increasing temperature.

3.3. Porosity & Initial Saturation

The results of porosity and initial mixed saturation S_{tot}^{i} measurements discussed in @ are given in Table 3-1 and Table 3-2.

scalar →	$\rho^{c.s\ dry}$	$\rho^{c.s\ wsat}$	n	S_{tot}^{i}
unit →	(g/cm^3)	(g/cm^3)	[-]	[-]
batch 1	1.673	1.992	0.320	40%
batch 2	1.670	2.001	0.331	39%
batch 3	1.665	1.991	0.326	42%
avg	**1.67**	**1.99**	**0.325**	**40%**

Table 3-1: Porosity and initial mixed saturation results from measurements based on dry NAPL free sand

scalar →	ρ_s^{i}	$\rho^{c.s\ wsat}$	n	S_{tot}^{i}
unit →	(g/cm^3)	(g/cm^3)	[-]	[-]
batch 1	1.800	1.995	0.325	40%
batch 2	1.801	1.999	0.325	39%
batch 3	1.801	1.991	0.325	41%
avg	**1.80**	**2.00**	**0.325**	**40%**

Table 3-2: Initial mixed saturation results from measurements based on sand carrying initial mixed saturation

The average porosity of the sand in the columns was 32,5 % while the approximate S_{tot}^{i} was 40%.

Using this value of the porosity, the volume of water added in the sand to full saturation S_w^+, the amount of additional pure phase NAPL M_{NAPL}^{+} (and V_{NAPL}^{+}) and the dimensions of the porous medium in the columns, the additional NAPL saturation S_{NAPL}^{+} was calculated. Also the initial mixed saturation S_{tot}^{i} was verified.

[6] within the studied range (15 - 50 °C)

		C1	C2
n	-	0.325	0.325
$I.D.^{columns}$	(cm)	8	8
h_{sand}	(cm)	8	8
V_{column}^{total}	(cm^3)	402.1	402.1
V_{void}^{total}	(cm^3)	130.7	130.7
V_w^+	(ml)	78	80
S_w^+	%	59.7%	61.2%
S_{tot}^i	%	40.3%	38.8%
M_{NAPL}^+	(gr)	36.976	36.934
V_{NAPL}^+	(ml)	36	36
ρ_{NAPL}	(gr/cm^3)	1.027	1.026
S_{NAPL}^+	%	27.5%	27.5%

Table 3-3: Results of additional NAPL saturation (S^+_{NAPL}) calculation (V_w^+: water volume added to full saturation, S_w^+: corresponding increase of water saturation, S_{tot}^i: Initial mixed saturation in sand samples, M_{NAPL}^+: additional drained mass of NAPL, V_{NAPL}^+: additional drained volume of NAPL, S_{NAPL}^+: additional saturation of NAPL besides the S_{NAPL}^i contained in the sand samples)

The initial NAPL saturation, i.e. the NAPL amount carried from the sand as extracted from field conditions was estimated based on the method discussed in Section 2.2.3b. The total mass loss from the sand samples due to evaporation is given in Figure 3.7 . The calculated results are given in Table 3-4.

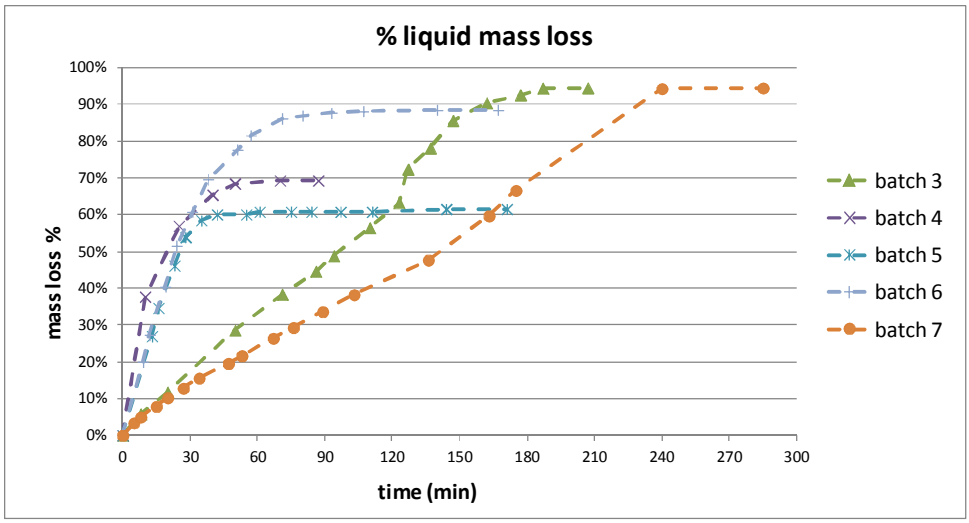

Figure 3.7: Liquid mass loss from sand samples

batch	min S^i_{NAPL}%	max S^i_{NAPL}%	S^i_{NAPL}%
1	11.8%	14.1%	13.0%
2	12.1%	13.8%	12.9%
3	15.2%	17.9%	16.5%
4	9.1%	10.7%	9.9%
5	10.6%	13.3%	11.9%
avg	**11.8%**	**14.0%**	**12.9%**

Table 3-4: Results of Initial NAPL saturation estimation

Summarising the results for the two column experiments, the pore space of the porous media amounted 32,5% of the total volume. Within this pore space an approximate 40% mixed saturation was already contained as the sand was collected from field conditions. This 40% consisted of an estimated 13% of NAPL phase (S^{i}_{NAPL}) and the rest of water phase. The 60% pore space which initially, i.e. after packing, was covered by air was saturated with water phase producing a two phase system with approximately 13% NAPL and 87% water. The NAPL amount drained in both the columns corresponded to 27.5% saturation. This replaced water saturation producing a two phase system with macroscopic saturations of approximately 40% NAPL ($S^{\max}_{NAPL}$) and 60% water.

3.4. Column experiment

The NAPL phase did not breakthrough during the drainage phase; the product of this phase was entirely aqueous. As the mass balance could only be covered by the ponded NAPL on top of the sand and the phase ended at the point when all the ponded NAPL was depleted, the amount of water outflow was equal to the additional NAPL amount, i.e. 36ml. That was the case for both columns as the procedure followed was identical. At the end of the drainage phase the macroscopic NAPL saturation of both the columns reached its maximum level, i.e. the $S^{\max}_{NAPL}$, of approximately 40%. This maximum macroscopic NAPL saturation remained constant until the moment of NAPL breakthrough.

The imbibition phase started with the following approximate fractions of saturations: 40% NAPL phase and 60% water phase, corresponding to 52.3 and 78.4 ml respectively. From the beginning of this phase, the bottom outflow was covered by water entering the sand from the top boundary. At the first step of this phase a water head of 2 cm corresponding to a volume of 100.5 ml was let depleted. The equal produced volume was completely aqueous for both columns. The aqueous product (100.5 ml) amounted more the initial water fraction of the pore volume (78.4 ml). This leads to the conclusion that water phase broke through the NAPL body with the macroscopic saturation of NAPL remaining at the maximum, i.e. $S^{\max}_{NAPL}$. At the intermediate low pressure step followed only at column 1, a water head of 2cm was again let depleted, this time under slightly higher pressure conditions (see Section 2.2.2b) and similarly this produced a volume of 100.5 ml water phase only. This indicated the fact that the wetting phase of the system was well connected between the ponded at the top boundary and outflow at the bottom boundary.

Production continued being entirely aqueous for both columns at the beginning of the next high constant pressure imbibition step (see Section 2.2.2b). NAPL eventually broke through at column 1, which previously followed an additional low pressure imbibition step, after 1 more pore volume of water was produced (approx. 130 ml). At column 2, NAPL broke through after 3 more pore volumes of water phase were produced (approx 390 ml). In total, the NAPL phase broke through after approximately 2,5 (330ml) and 3,7 (490 ml) pore volumes of water were produced respectively for columns 1 and 2 from the start of the imbibition phase.

The NAPL breakthrough brought the phase of maximum macroscopic NAPL saturation ($S^{\max}_{NAPL}$ 40%) to an end. NAPL production was similarly low for both columns right from the beginning, amounting a maximum of hardly 2 % of the pore volume at the first 2 pore volumes produced after NAPL breakthrough. At that point the total flow rate minimised. The already low NAPL production

gradually dropped for both columns for the following pore volumes produced with a parallel increase of the total flow rate, reaching an approximately constant equilibrium low level, point when the residual NAPL saturation (S_{NAPL}^{res}) target was accomplished. At this point the total mass of NAPL recovered was 25.3 g for column 1 and 21.4 g for column 2, corresponding to a drop of NAPL saturation from the $S_{NAPL}^{\max}$ (approx. 40%) of 19 and 16 % respectively.

The product of the experiment, right from the moment of NAPL breakthrough, was an emulsified mixed liquid consisting primarily of water phase. Even at the point when NAPL production was maximised the NAPL fraction of the mixed product hardly reached a 2%. The emulsified product is illustrated in the following pictures.

Figure 3.8: Mixed product right after NAPL breakthrough (left) and during NAPL-water separation process (right)

During the warming phase, NAPL production dropped even more for both columns; in fact it followed a decreasing trend. For column 2 in particular it reached zero at the 6th pore volume and remained at that level for the rest of the warming phase, amounting 3 pore volumes of completely NAPL-free aqueous product. At the same time flow rate approximately doubled following the decrease of water viscosity due to the elevated temperature.

During the temperature restoration phase, with the temperature back at ambient (21°C), the production of column 1 increased right from the start and remained approximately constant during the phase whole phase (8 pore volumes). However it remained below the equilibrium level of S_{NAPL}^{res}, i.e. level before the start of warming, and certainly at an extremely low level compared to the respective water production. For column 2, production of NAPL remained zero for the first 4 of the total 8 pore volumes, before some extremely low NAPL outflow restarted.

Finally, during the cooling phase, for column 1 the NAPL production continued rising finally reaching the S_{NAPL}^{res} equilibrium production level. For column 2 it persisted at the same level as of the last pore volumes of the preceding phase of restored temperature. Naturally, during this phase the flow rate in both columns dropped following the increase of water viscosity.

The produced NAPL mass per experimental phase for the two columns is shown in Figure 3.9 and Figure 3.10.

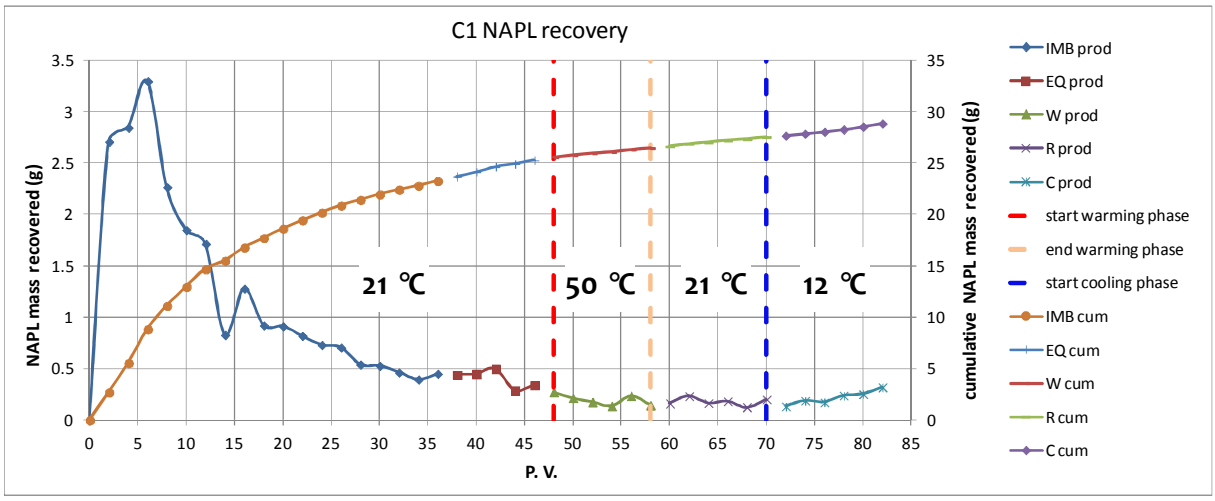

Figure 3.9: NAPL recovery per double P.V. for Column 1 (C1)

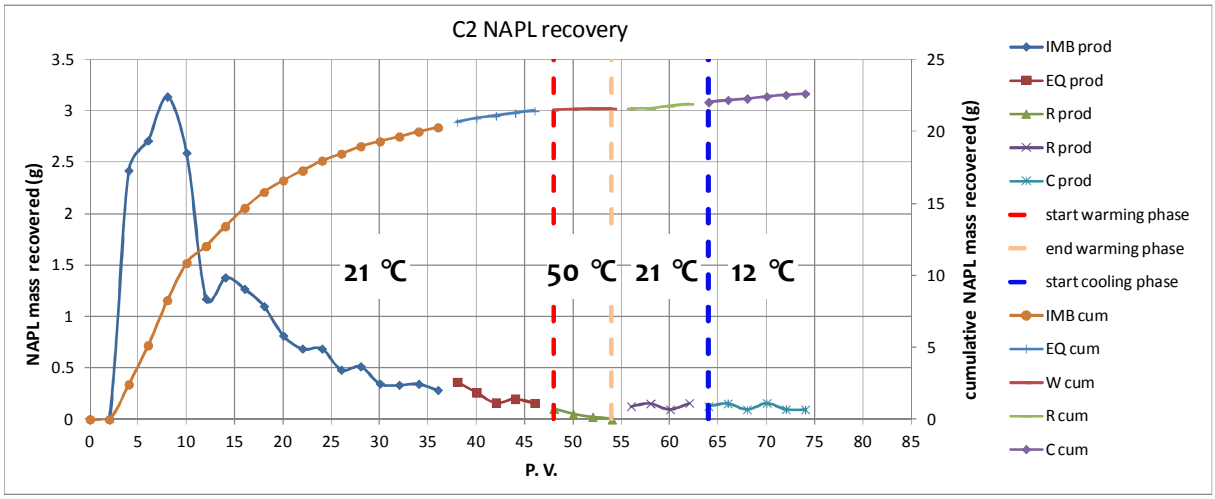

Figure 3.10: NAPL recovery double P.V. for Column 2 (C2)

The drop of NAPL saturation for the two columns expressed with the initial NAPL saturation S^{i}_{NAPL} as a base value is given in Figure 3.11 and Figure 3.12.

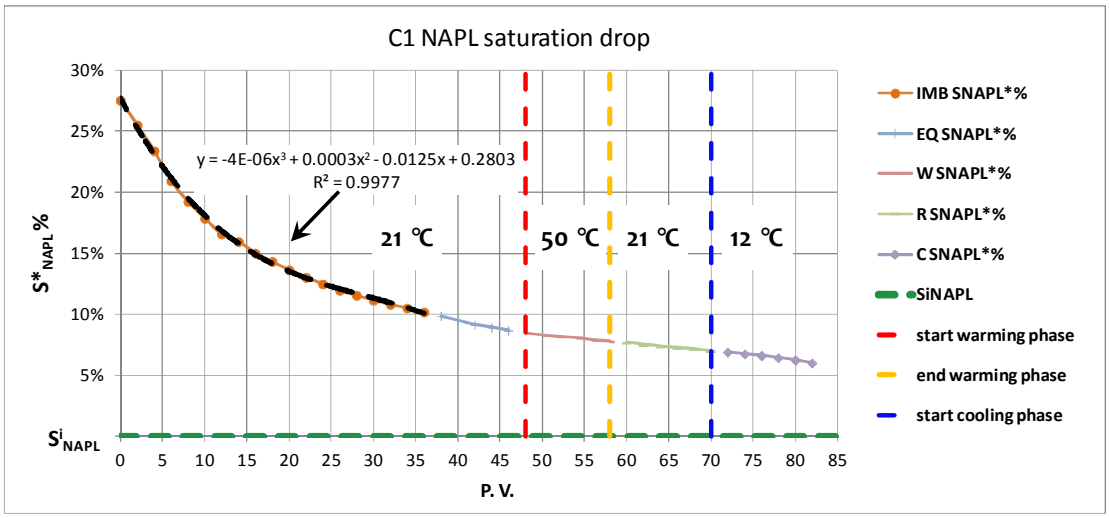

Figure 3.11: Saturation drop for Column 1 (C1) (S^{i}_{NAPL} approx. 13%)

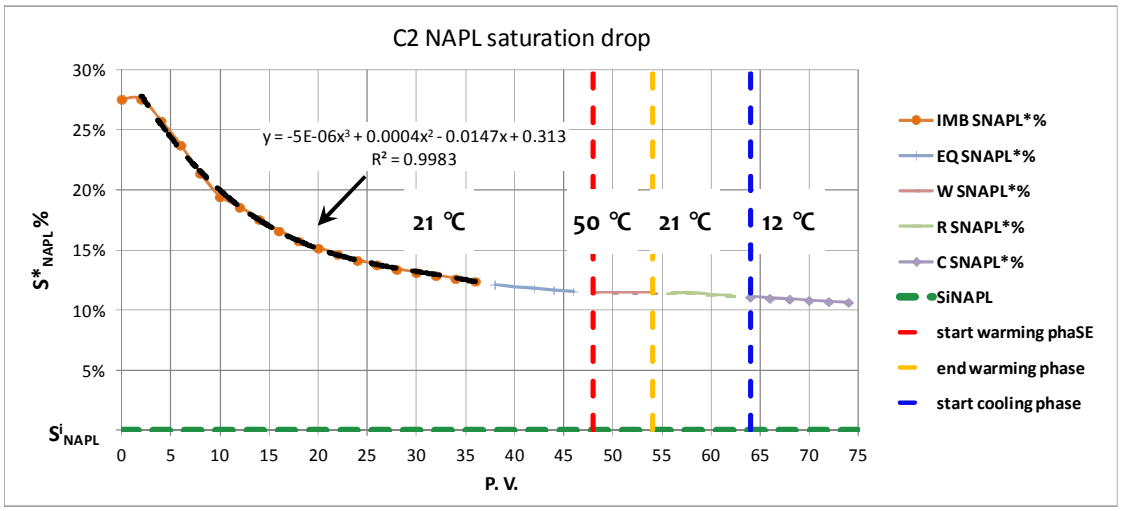

Figure 3.12: Saturation drop for Column 2 (C2) (S^i_{NAPL} approx. 13%)

The comparison of the NAPL production and NAPL saturation drop is given in Figure 3.13 and Figure 3.14.

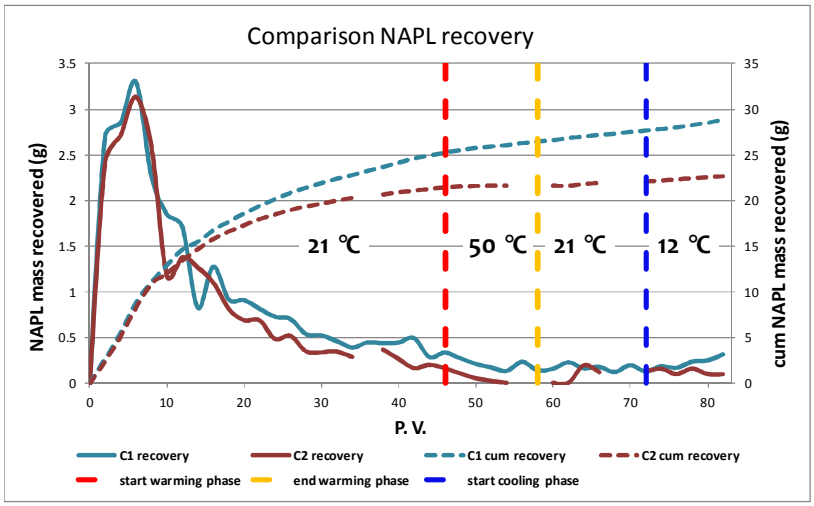

Figure 3.13: Comparison of NAPL recovery for the two experiments

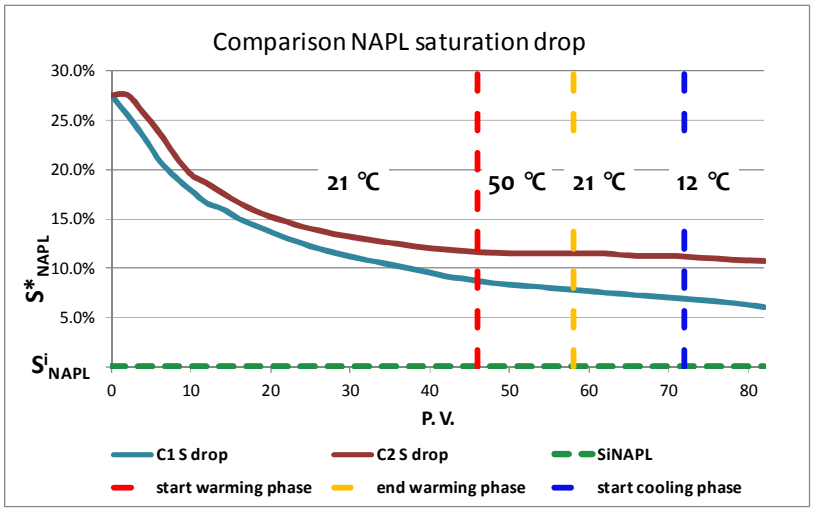

Figure 3.14: Comparison of NAPL saturation drop for the two experiments (S^i_{NAPL} approx. 13%)

An impression of the change of the NAPL production is given in the following pictures (Figure 3.15) starting from the equilibrium S_{NAPL}^{res} production.

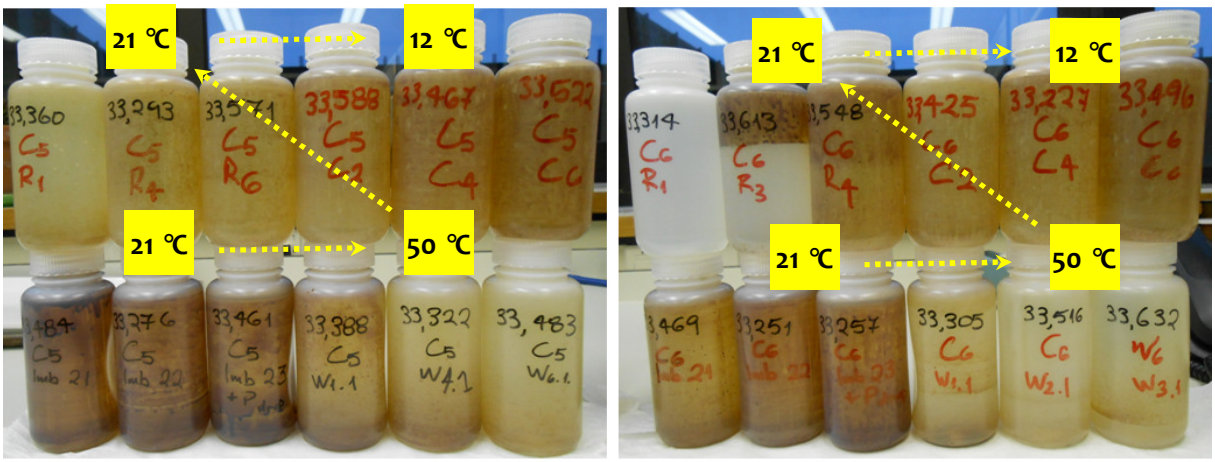

Figure 3.15: Impression of variation in NAPL production (C5: Column 1, C6: Column 2, Imb: Imbibition phase, W: Warming phase, R: Restored temperature phase, C: Cooling phase)

The flow rates of the non-wetting phase during drainage and of the wetting phase during the temperature variation phase, i.e. with the non-wetting phase at residual saturation, are given in Table 3-5 and Figure 3.16 for the two experiments (C1 and C2) together with the viscosity ratios (M) of the two fluids.

		drainage	C1 imbibition			C2 imbibition		
T	(°C)	21	12	21	50	12	21	50
Q	(cm3/sec)	0.3	0.28	0.36	0.66	0.33	0.43	0.78
q	(cm/sec)	6.0E-03	5.5E-03	7.2E-03	1.3E-02	6.5E-03	8.5E-03	1.6E-02
v	(cm/sec)	1.84E-02	1.7E-02	2.2E-02	4.1E-02	2.0E-02	2.6E-02	4.8E-02
σ	(dynes/cm)	30	32	30	18	32	30	18
μ^{w}	(mPasec)	1.00	1.31	1.00	0.55	1.31	1.00	0.55
μ^{NAPL}	(mPasec)	10.9	17.2	11.0	4.5	17.2	11.0	4.5
Ca	(-)	3.1E-04	3.1E-05	3.4E-05	5.6E-05	3.6E-05	4.0E-05	6.6E-05
M	(-)	10.9	7.6E-02	9.1E-02	1.2E-01	7.6E-02	9.1E-02	1.2E-01
logC	(-)	-3.5	-4.5	-4.5	-4.3	-4.4	-4.4	-4.2
logM	(-)	1.0	-1.1	-1.0	-0.9	-1.1	-1.0	-0.9

Table 3-5: Capillary numbers and viscosity ratios during drainage and imbibition phases (21 °C refers to the restoration phase between the warming and cooling phases)

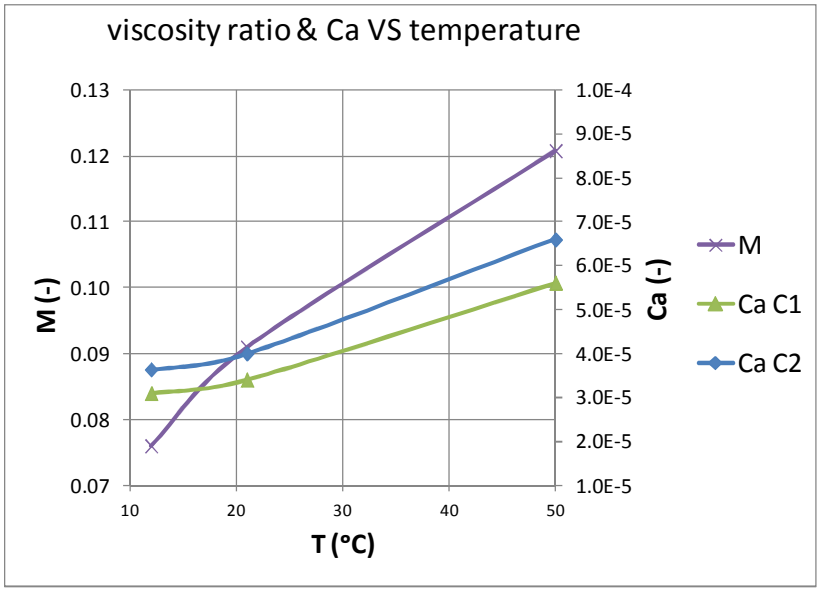

Figure 3.16: Viscosity ratio and Capillary number vs temperature for the two experiments (C1 & C2) (21 °C refers to the restoration phase between the warming and cooling phases)

The distribution of end NAPL saturation was studied based on cross sections of the porous medium (see Figure 3.17 and Figure 3.18). These cross sections show that residual saturation was not uniformly distributed, but some areas containing entrapped NAPL contribute significantly to the total fraction of NAPL saturation compared to the rest of the total pore volume. In particular, in both experiments a significant amount of NAPL is trapped at or right below the porous medium top surface.

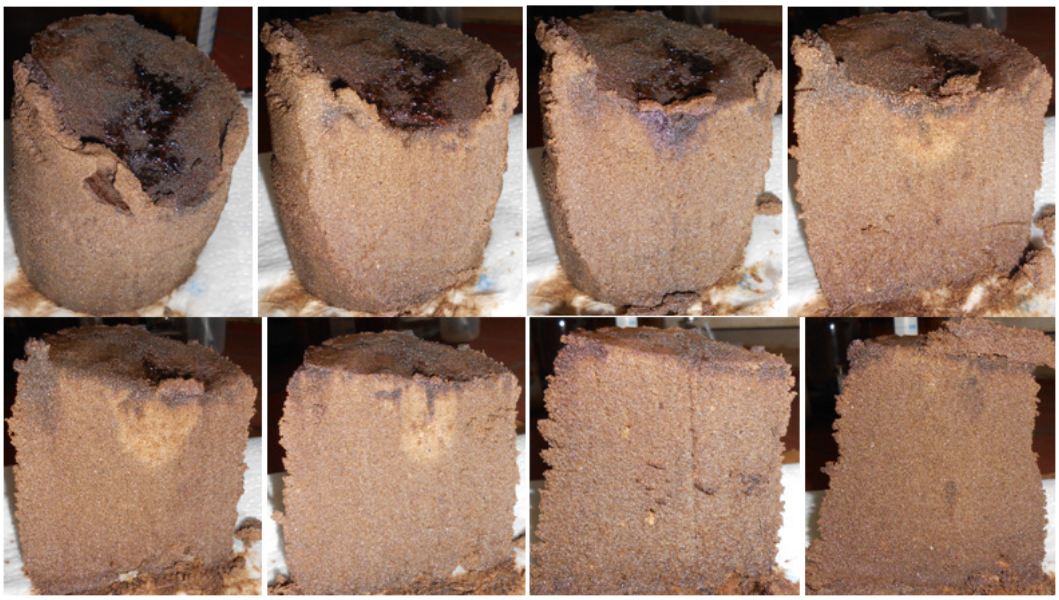

Figure 3.17: Cross sections of porous medium of 1st experiment (C1)

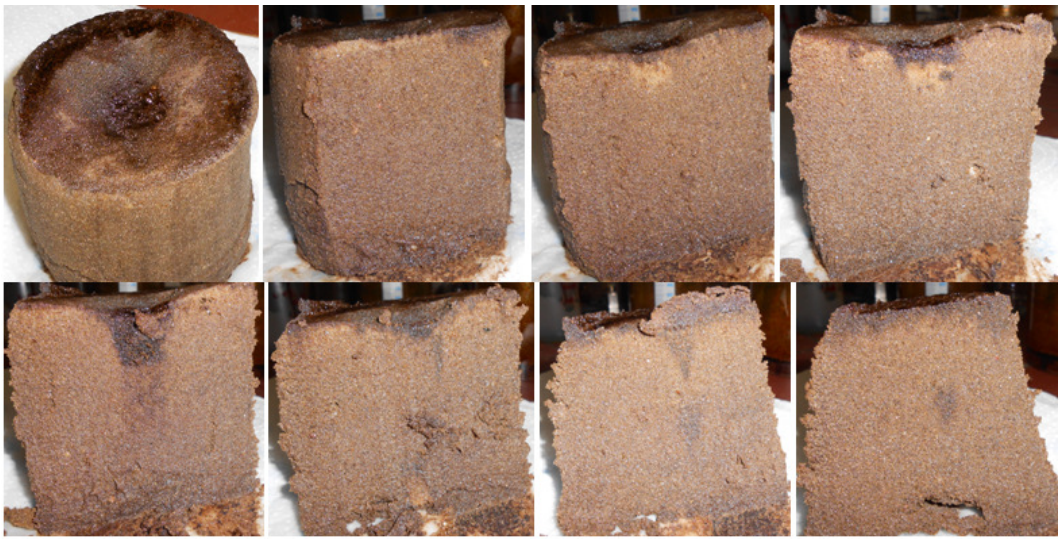

Figure 3.18: Cross sections of porous medium of 2nd experiment (C2)

4. DISCUSSION

The wettability test proved that the porous medium under research has remained water-wet despite the long term exposure to the oil-gas tar type NAPL. This fact is of significant importance regarding the distribution of the end/irreducible NAPL saturation. Moreover it allows the residual NAPL saturation to be lower compared to the case of a NAPL wet system. It was assumed that the water wet conditions remained practically unchanged within the temperature variation range of this experimental research.

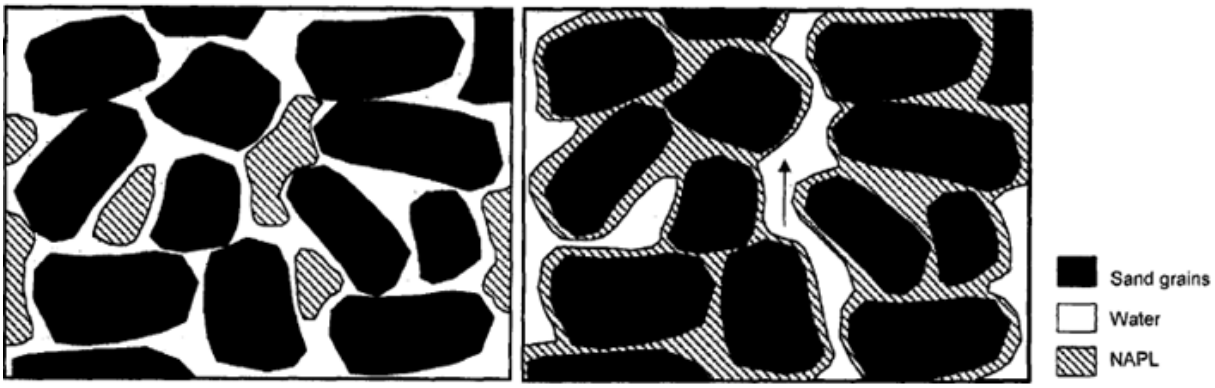

Figure 4.1: NAPL distribution following water flooding for water-wetting case (left) and NAPL-wetting case (right) [10]

The interfacial tension measurements concluded a value of approximately 31 and 30 dynes/cm for temperature of 15 °C and 21 (ambient laboratory temperature) respectively. A comparison of these values with values of interfacial tension reported in literature is given in the following table.

NAPL	source	γ (dynes/cm)
Amersfoort oil	present study	**29**
PCE	[Sleep et al.]	**45**
Voltesso	[Sleep et al.]	**42**
Strasbourg coal tar	[Villaume et al.]	**22**
Coal tar 1	[Hugaboom et al.]	**13**
Coal tar 2	[Hugaboom et al.]	**20**
Creosote	[Hugaboom et al.]	**9.5**
Soltrol-130	[Wilson et al.]	**48**
Kerosene	[Wilson et al.]	**38.5**
gasoline	[Wilson et al.]	**23**
p-xylene	[Wilson et al.]	**36**
PCE	[Wilson et al.]	**42**
carbon tetrachloride	[Wilson et al.]	**33**

Table 4-1: Comparison of interfacial tension of "Amersfoort oil" with literature values

The measurements of interfacial tension at different temperatures concluded that a rise of temperature from the average subsurface temperature of 15 °C to a temperature of 50 °C results in an approximate 40% drop of interfacial tension. This level of drop indicates that interfacial tension with a variation of temperature remains within the same order of magnitude. This is in contrast to the drop of interfacial tension achieved with the use of chemicals (surfactants) which reduces the order of magnitude of interfacial tension. For example, Pennell et al. [8] report a drop

of PCE-water interfacial tension from 47.8 to 0.09 dynes/cm achieved with the use of different surfactant solutions.

The correlation of the change of interfacial tension with temperature with the respective change in densities of the two fluid phases (water and NAPL) concluded that the new equilibrium between the gravitational driving force and the resisting capillary forces at the target temperature of 50 °C is more unfavourable than the equilibrium at 15 °C (average sub-surface temperature in the Netherlands), assuming that the contact angles are not significantly affected by that temperature variation.

In the column experiments, NAPL saturation started at approximately 13 %. This initial saturation was increased by draining an additional amount of pure phase NAPL at approximately 40%. This drainage process can be described as a secondary drainage. Drainage was carried out with a capillary number of the order of magnitude of 10^{-4} (see Table 3-5). Given this order of magnitude and the viscosity ratio of the NAPL and water phases, on the basis of the phase diagram for immiscible displacement of Lenormand et al. [5] the drainage process can be described by a low capillary number (Nca) with an intermediate to high viscosity ratio (M). This combination probably led to a capillary fingering type displacement. This conclusion agrees with the delay in NAPL phase breakthrough.

The imbibition process started before NAPL breakthrough, i.e. with NAPL macroscopic saturation at the maximum level of approximately 40%. The capillary number at that temperature level (at 21 °C) was measured at the order of magnitude of 10^{-5} (see Table 3-5). Given the fact that during the start of water phase imbibition NAPL saturation in the column was at its maximum, therefore restricting the water phase flow rate considerably, the capillary number of that phase can be assumed lower than 10^{-5}. With an inverse viscosity ratio compared to the drainage process, the water phase probably imbibed in a viscous fingering pattern. In this way the ease of water breakthrough through the maximum NAPL saturation (40%) can be explained. In Figure 4.2 the two processes, i.e. drainage and imbibition, are illustrated on the phase diagram of Lenormand for immiscible displacement.

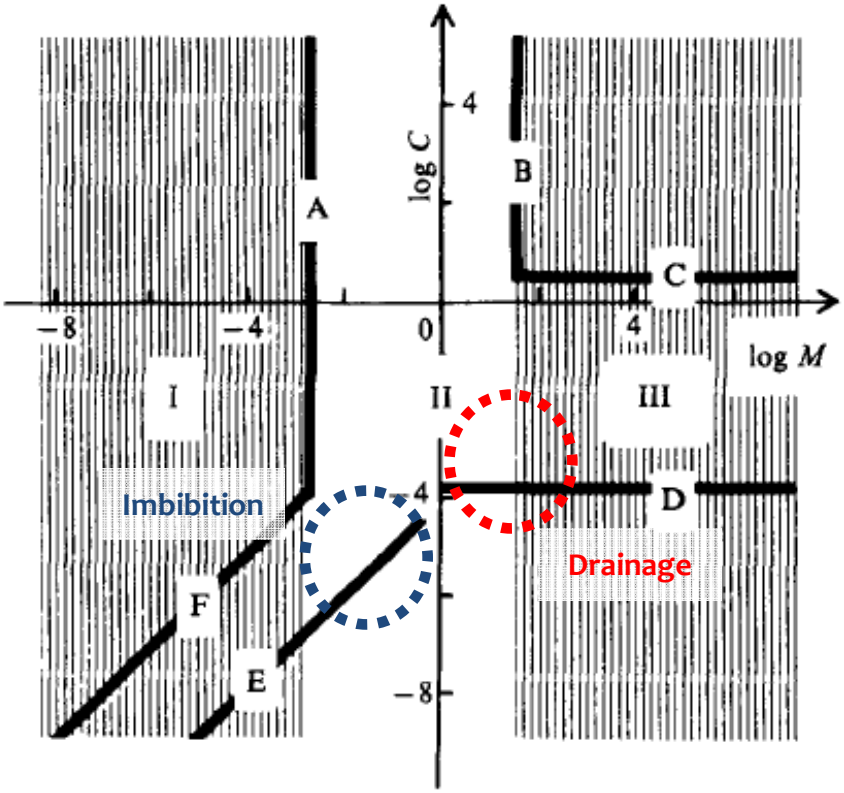

Figure 4.2: Drainage and imbibition processes on Lenormand phase diagram [5]

Based on the nature of the experimental product at the point of NAPL breakthrough, it can be inferred that NAPL phase was already disconnected and the water phase occupying around 60% of the total saturation was flowing completely connected. The NAPL phase was not yet immobile because its high saturation (approx. 40%) allowed the combination of the (low) density difference and imposed flowing wetting phase pressure gradient to exceed the entry pressures at the pore constrictions and drive some disconnected NAPL bodies downward to the outflow of the column. However, given the viscosity difference of the two phases, NAPL was unable to compete with the flow rate of the significantly less viscous water phase. This resulted in extremely low NAPL production. Especially as NAPL saturation dropped, NAPL production approached zero, compared to water phase production. The low recovery rates were expected based on the properties of the particular type of NAPL. The combination of high viscosity and low gravitational forces (density close to that of water) cause capillary forces to be more important in these systems than for other DNAPL types such as chlorinated solvents[7], governing both the initial DNAPL infiltration process and the final distribution of DNAPL after redistribution or recovery [10] .

The point where NAPL saturation can be regarded as residual is arbitrary. In this case NAPL saturation was considered residual when the NAPL production per P.V. of total product stabilised one order of magnitude lower than the maximum NAPL production per P.V. At that point the macroscopic NAPL saturation amounted approximately 20 - 25%. This was the starting point for the phase of limited warming. At the increased temperature, given the changes in water phase viscosity and interfacial tension, the capillary number (Nca) was almost doubled (see Table 3-5). However the capillary number (Nca) did not change order of magnitude. The clear decrease in

[7] Chlorinated solvents are significantly denser and equally or less viscous than water

gravitational driving forces, expressed by the Bond number (Nbo), based on the change of density difference and interfacial tension, resulted in further drop of NAPL production. Possible effects of the increase in Capillary number (Nca) on the microscopic NAPL saturation distribution could not possibly be evaluated given the nature of the experiment.

During the two phases following the warming phase, i.e. temperature first restored at 21°C and subsequently lowered at 12°C, the Bond number (Nbo) increased and the Capillary number (Nca) decreased. These phases did not result in a significant change of NAPL production, given also the fact that the columns were already exhausted from the vast number of circulated pore volumes of water phase; however the fact that a small increase was recorded can establish the importance of gravitational forces for NAPL production. This effect is clearer in Column 2 (see Figure 3.15).

The main difference between the two experiments was the increased wetting phase flow rate during the beginning of imbibition. The results showed that the end macroscopic NAPL saturation for the column with the higher wetting phase flow rate was higher, yet the water phase flow rate at the end of the experiment was also higher. This fact can be linked to the manner the wetting phase displaced NAPL, taking over pore space and creating wetting phase flow paths. Differences in imbibition conditions may lead to different NAPL entrapment conditions and spatial distribution of residual NAPL saturation. The comparison of NAPL recovery and saturation drop for the two experiments is given in Figure 3.13 and Figure 3.14 respectively.

Based on the study of the porous media cross sections (see Figure 3.17 and Figure 3.18) in both experiments a significant amount of NAPL is trapped at or right below the porous medium top surface. This fact indicates that once the water (wetting) phase took over during imbibition, even these larger NAPL bodies became unable to overcome the entry pressures and drain further downwards. Further, in the second experiment (C2) an amount of NAPL remained trapped close to the bottom boundary indicating possible boundary effects. The contribution of this particular entrapped NAPL saturation to the total end macroscopic NAPL saturation could not be quantified.

The level of residual NAPL saturation (approx. 20 – 25 %) of this experimental research corresponds to the particular drainage and imbibition processes carried out during the experiment. Furthermore the study of the end cross sections of the porous media revealed the importance of boundary effects which increase the total macroscopic NAPL saturation. To the contrary the particular experimental porous media were imposed to thorough water flushing, lowering NAPL saturation. In field conditions apart from the differences in drainage and imbibition process, the NAPL migration and entrapment are largely determined by the in situ heterogeneities. Moreover, the surrounding water phase is flowing at aquifer velocities, i.e. much lower than the flow velocities during the experimental water flushing. These differences should be taken into account before correlating the level of the particular experimental residual saturation with the respective in situ. The goal of the experiment was not to match the level of residual saturation existing in situ but to create residual NAPL conditions which would allow the evaluation of the effect of limited warming.

5. CONCLUSIONS

The main conclusion of the present research was that for the particular water-wet 2-phase system limited warming cannot function as a remobilisation factor for residual NAPL saturation. With an increase of temperature from 15 to 50 °C the interfacial tension between this tar type NAPL and water drops by approximately 40% however the decrease in density difference between the two phases is higher leading to a more unfavourable equilibrium.

The increase in capillary number (effect of viscous forces) by a factor 2, as a consequence of the drop of the viscosity of the flowing wetting phase and the drop of interfacial tension, parallel to the decrease of Bond number (effect of gravitational forces) produces no favourable effect in regards to macroscopic saturation.

The main difference between the two experiments, i.e. difference in Capillary number at the start of imbibition, may have resulted in differences in magnitude and distribution of NAPL residual saturation; however the nature of the experiments does not allow further quantification.

NAPL production was extremely low reasoned by the relative properties of the two liquids (viscosity, density). It is uncertain whether different drainage conditions and/or higher initial NAPL saturation (starting point) than the approximate 40% of this research could lead to higher production rates at this level of saturation.

Finally, the level of residual NAPL saturation (20 – 25 %) produced in both experiments cannot be engaged as representative for the in-situ conditions. The in situ drainage and imbibition conditions as well as the in situ heterogeneities, factors responsible for the magnitude and distribution of residual NAPL saturation were unknown and therefore not modelled in the experiment.

As a general remark, the present research looked into the response of residual phase oil-gas tar to limited warming. It was based on an actual contamination case hence it studied the behaviour of specific materials. Despite the fact that the main target of the experimental work was accomplished, i.e. to evaluate weather limited warming can trigger remobilisation, there is a number of issues which would definitely require additional investigation. These are listed below as recommendations for additional research.

1. Effect of temperature on contact angles of sand-water-oil-gas tar. Corresponding effects on mobility and entrapment mechanisms of oil-gas tar.
2. Numerical investigation of drainage and imbibition processes. Resulting patterns of NAPL migration and distribution under different conditions (e.g. flow rates, initial NAPL saturation).
3. Effect of cooling if applied directly after NAPL immobilisation. To what extend can the favourable new equilibrium resulting from cooling have a positive effect on residual NAPL saturation?
4. Micro-scale investigation of oil-gas tar trapping mechanisms; behaviour of residuals during water flooding.
5. Minimum oil-gas tar saturation for efficient recovery at field conditions.

Bibliography

[1] R. M. Cohen, J. W. Mercer, M. Slenska and M. Brourman, "Creosote Wettability Review and Evaluation at a Portion of the Cabot Carbon/Koppers Superfund Site," Niagara Falls, NY, 2007.

[2] A. S. Mayer and M. S. Hassanizadeh, Soil and Groundwater Contamination: Nonaqueous Phase Liquids, Washington, D.C.: American Geophysical Union (AGU), 2005.

[3] A. S. Mayer and C. T. Miller, "An Experimental Investigation of Pore-Scale Distributions of Nonaqueous Phase Liquids at Residual Saturations," *Transport in Porous Media,* vol. 10, pp. 57-80, 1993.

[4] F. Gioia and M. Urciuolo, "Combined effect of Bond and capillary numbers on hydrocarbon mobility in porous media," *Journal of Hazardous Materials,* no. B133, pp. 218-225, 2006.

[5] R. Lenormand, E. Touboul and C. Zarcone, "Numerical models and experiments on immiscible displacements in porous media," *Journal of Fluid Mechanics,* vol. 189, pp. 165-187, 1988.

[6] J. L. Wilson, S. H. Conrad, W. R. Mason, W. Peplinski and E. Hagan, Laboratory Investigation of Residual Liquid Organics, United States Environmental Protection Agency, 1990.

[7] B. E. Sleep and Y. Ma, "Thermal variation of organic fluid properties and impact on thermal remediation feasibility," *Journal of Soil Contamination* , vol. 6, no. 3, pp. 281-306, 1997.

[8] K. D. Pennell, G. A. Pope and L. M. Abriola, "Influence of Viscous Forces on the Mobilization of Residual Tetrachloroethylene during Surfactant Flushing," *Environmental Science & Technology,* vol. 30, no. 4, pp. 1328-1335, 1996.

[9] K. M. Ng, H. T. Davis and L. E. Scriven, "Visualisation of Blob Mechanisms in Flow through Porous Media," *Chemical Engineering Science,* vol. 33, pp. 1009-1017, 1978.

[10] D. A. Hugaboom and S. E. Powers, "Recovery of Coal Tar and Creosote from Porous Media: The Influence of Wettability," *Ground Water Monitoring & Remediation,* vol. 22, no. 4, pp. 83-90, 2002.

[11] L. N. Reddi and H. Wu, "Mechanisms Involved in Vibratory Destabilization of NAPL Ganglia in Sands," *Journal of Environmental Engineering,* vol. 122, no. 12, pp. 1115-1119, 1996.

[12] K. Singh, R. K. Niven, T. J. Senden, M. L. Turner, A. P. Sheppard, J. P. Middleton and M. A. Knackstedt, "Remobilization of Residual Non-Aqueous Phase Liquid in Porous Media by Freeze-Thaw Cycles," *Environmental Science & Technology,* vol. 45, pp. 3473-3478, 2011.

[13] S.Gkekas, "Amersfoort Vetgasvabriek: Field research summary and actions planning," s.b.n.s. / Utrecht University, Utrecht, 2013.

[14] s.b.n.s., "Archive," 2013.

[15] S. M. J. B. T. J. McCutcheon, "Water Quality," in *Handbook of Hydrology*, New York, McGraw-Hill, 1993.

[16] W. B. Tucker, in *Surface Tension by Pendant Drops*, Massachusetts Institute of Technology, 1938, pp. 26-90.

[17] F. K. Hansen and G. Rodsrud, "Surface Tension by Pendant Drop," vol. 141, no. 1, 1990.

[18] S. Fritz, "Experimental Investigations of Water Infitration into Unsaturated Soil - Analysis of Dynamic Capillary effects," University of Stuttgart, Stuttgart, 2012.

[19] C. Cottin, H. Bodiguel and A. Colin, "Drainage in two-dimensional porous media: From capillary fingering to viscous flow," *The American Physical Society*, 2010.

[20] J. F. Villaume, P. C. Lowe and D. F. Unites, "Recovery of Coal Gasification Wastes: An innovative Approach".

APPENDICES

I. Pressure and head diagrams

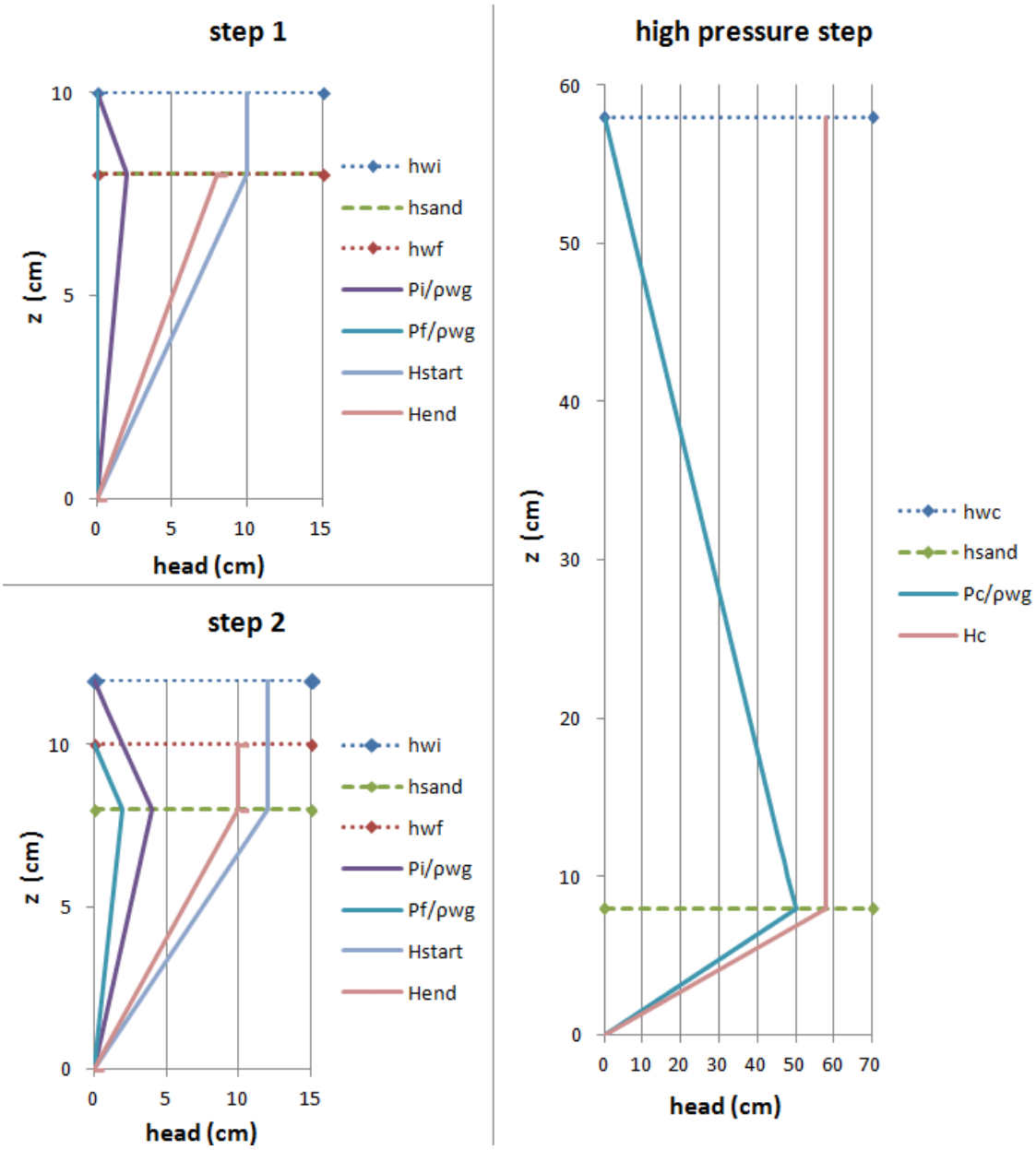

I.1 Pressure and head formulation of imbibition phases (P_{atm} taken as zero pressure condition)

II. Interfacial tension measurement-pendant drops profiles

T (ºC) →	16	22	30	38	49
avg Ro (m)	3.32E-03	3.39E-03	3.61E-03	3.80E-03	4.04E-03
avg Ds (m)	3.11E-03	3.16E-03	3.26E-03	3.31E-03	3.21E-03
avg De (m)	6.40E-03	6.69E-03	7.11E-03	7.46E-03	7.88E-03
avg Ds/De	4.86E-01	4.72E-01	4.59E-01	4.43E-01	4.08E-01
avg β [-]	1.16E-01	1.08E-01	1.01E-01	9.34E-02	7.70E-02
avg Ro (mm)	3.320	3.395	3.613	3.800	4.035
ρw (kg/m3)	998.972	997.800	995.678	992.997	988.513
ρw (g/cm^3)	0.999	0.998	0.996	0.993	0.989
ρnapl (kg/m^3)	1033	1026.313	1017.781	1009.250	997.520
ρnapl (g/m^3)	1.0327	1.0263	1.0178	1.0093	0.9975
Δρ (kg/m3)	33.739	28.512	22.103	16.253	9.007
Δρ (g/cm3)	0.034	0.029	0.022	0.016	0.009
Υ (N/m)	0.0314	0.0297	0.0280	0.0247	0.0187
Υ (Dynes/cm)	31.4	29.7	28.0	24.7	18.7

II.1 Intefacial tension results

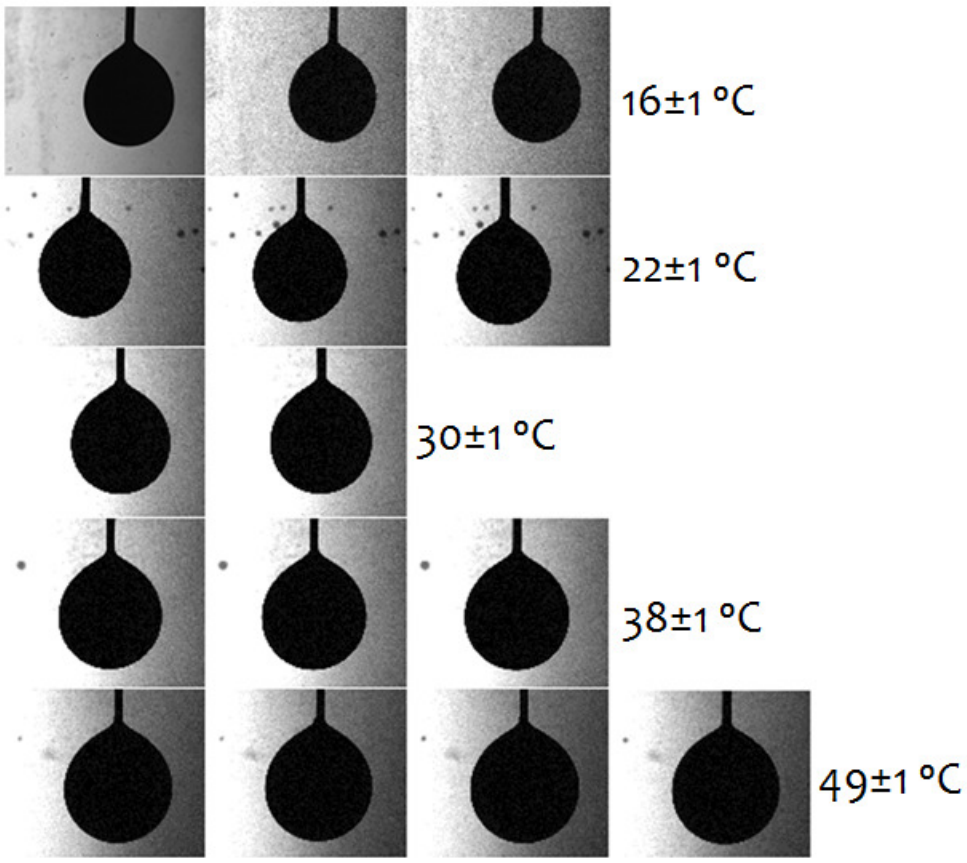

II.2 Pendant drops profiles

III. Wettability test-sessile drops

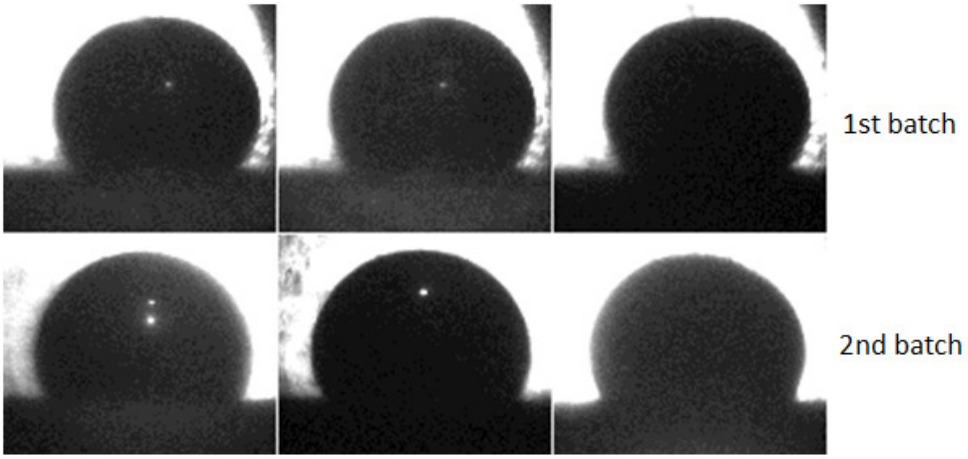

III.1 Sessile drops profiles

IV. LNAPL observations

IV.1 LNAPL observations at the end of the experiments

V. Miscellaneous

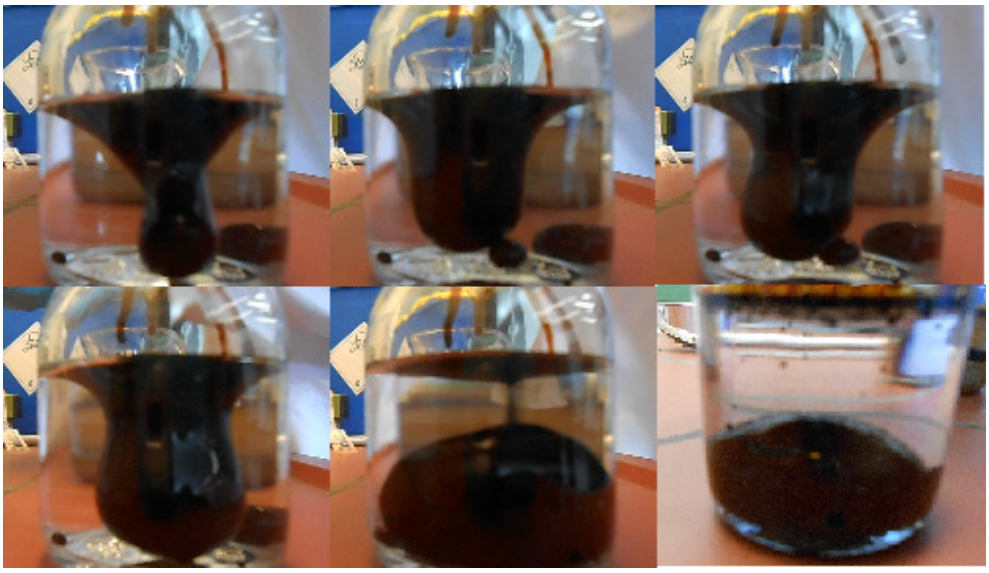

V.1 Oil-gas tar in water